DOT/FAA/TC-17/31

Federal Aviation Administration
William J. Hughes Technical Center
Aviation Research Division
Atlantic City International Airport
New Jersey 08405

Development of Sonic Infrared Inspection Technology for Nondestructive Evaluation of Critical Aircraft Engine Rotating Components

September 2017

Final Report

U.S. Department of Transportation
Federal Aviation Administration

NOTICE

Technical Report Documentation Page

1. Report No.	2. Government Accession No.	3. Recipient's Catalog No.
DOT/FAA/TC-17/31		

4. Title and Subtitle	5. Report Date
DEVELOPMENT OF SONIC INFRARED INSPECTION TECHNOLOGY FOR NONDESTRUCTIVE EVALUATION OF CRITICAL AIRCRAFT ENGINE ROTATING COMPONENTS	September 2017
	6. Performing Organization Code

7. Author(s)	8. Performing Organization Report No.
John Polywoda	

9. Performing Organization Name and Address	10. Work Unit No. (TRAIS)
FTT America 1701 Military Trail Suite 110 Jupiter, FL 33458	
	11. Contract or Grant No.

12. Sponsoring Agency Name and Address	13. Type of Report and Period Covered
U.S. Department of Transportation Federal Aviation Administration Engine and Propeller Directorate 12 New England Executive Park Burlington, MA 018031	
	14. Sponsoring Agency Code ANE-111

15. Supplementary Notes

The FAA William J. Hughes Technical Center Aviation Research Division COR was Dave Galella.

16. Abstract

Detection of surface-breaking defects using fluorescent penetrant inspection (FPI) has been a well-established technique in the aerospace industry for many years. Though it has been used for many years, the FPI process has a number of shortcomings that still remain. One of the most critical is the high variability in inspection capability due to human factors. Dependence on the operator to make consistent observations and decisions can decrease its detection performance in the production shop environment. The sonic infrared (SIR) inspection method is an alternative nondestructive evaluation method to FPI.

This project aimed to develop tools to move the SIR technique closer to mainstream implementation. Methods for the development of artificial defects were evaluated. Methods relating to the improvement of defect recognition and characterization were evaluated for the automated identification of defects. Finally, the development of methods for the determination of the applicability of SIR to a given inspection task were generated, which would help users determine if Sonic IR is an applicable method and what testing and evaluation parameters are most suitable for a particular inspection task. This research brings SIR another step closer to successful depot implementation.

17. Key Words	18. Distribution Statement
Sonic IR, SIR, Nondestructive evaluation, Disk, Rotor, Artificial defects, Defect Recognition	This document is available to the U.S. public through the National Technical Information Service (NTIS), Springfield, Virginia 22161. This document is also available from the Federal Aviation Administration William J. Hughes Technical Center at actlibrary.tc.faa.gov.

19. Security Classif. (of this report)	20. Security Classif. (of this page)	21. No. of Pages	22. Price
Unclassified	Unclassified	83	

ACKNOWLEDGEMENTS

Important contributions to this work were made by Robert deLaneuville (Fatigue and Lifing, FTT), Ken Nelson (Senior Technician, Florida Turbine Technologies [FTT]), Dan Davies (Program Manager, FTT), David Sanabria (Mechanical Engineer, FTT), Steve Cargill (Consultant, Aerospace Structural Integrity), Michel Bode (Sandia National Laboratories), Andrea Dorado (Sandia National Laboratories), Jon Bartos (Consultant), and David Galella (Program Manager, FAA).

TABLE OF CONTENTS

LIST OF FIGURES

LIST OF TABLES

LIST OF ACRONYMS

AD	Artificial defect
AFRL	Air Force Research Laboratory
APU	Auxiliary power unit
DRA	Defect recognition algorithm
EDM	Electrical discharge machining
FOV	Field of view
FPI	Fluorescent penetrant inspection
FPS	Frames per second
FTT	Florida Turbine Technologies
MWIR	Mid-wave infrared
NDE	Nondestructive evaluation
NDT	Nondestructive testing
NUC	Non-uniformity correction
POD	Probability of detection
Q/A	Question/answer
Q factor	Quality factor
ROI	Region of interest
SIR	Sonic infrared
TiGA	Silver-filled epoxy
USAF	United States Air Force

EXECUTIVE SUMMARY

Detection of surface-breaking defects using fluorescent penetrant inspection (FPI) has been a well-established nondestructive testing (NDT) technique in the aerospace industry for generations. Though widely used, FPI has well-known intrinsic shortcomings that often lead to poor inspection reliability estimates (probability of detection or "POD") when evaluated in a realistic setting. The sonic infrared (SIR) inspection method displays much potential as an alternative NDT if it can be fully developed and implemented.

During the past few decades, many potential NDT methods have been the subject of exploratory development, but almost all have failed as they were passed from the laboratory to engineers in the practical world. Some had little potential to produce reasonable signal-to-noise ratios in a production environment, but others were not developed for practical use with a logical plan. The FAA and United States Air Force (USAF) have produced logical paths to implement SIR, and they are working in parallel to implement the method initially on flight turbine engine components. The initial focus by USAF is on rotor blades, whereas the FAA is concentrating its initial efforts on rotor disks (a more difficult, longer-term inspection subject). The FAA and the contractor team recognize that practical implementation on disks is a multiple-phase project with critical milestones along the way. This program has achieved success for several of those milestones.

SIR for crack detection is unique in that it requires true cracks or crack-like artificial defects (ADs) to rationally demonstrate the effectiveness of SIR. One objective for this program was to develop crack-like ADs that are much less expensive to insert into a component than fatigue cracks. This also provides the capability to insert artificial crack-like defects in component locations where it may be virtually impossible to produce cracks in the lab. To simulate a crack, the AD must produce an amplitude and heating/cooling characteristics that closely simulate a crack. This report shows some excellent achievements in this area, thereby lowering the cost of SIR implementation.

It is well-recognized that the inspector can be the most significant variable in manual performance of NDT. SIR is no exception. However, the physics of SIR offers the potential to automate the recognition of crack-like defects, at least to the point that allows the inspector to focus on a field of view that has been significantly reduced by the use of a defect recognition algorithm (DRA). One of the most significant developments of this program was an effort to combine the best technology of several promising approaches to provide a practical means to quickly search through volumes of data to recognize potential crack-like defects with a high inspection reliability. In fact, preliminary testing showed that the DRA can be as effective as manual inspection without inspector involvement to do a final evaluation.

A hybrid camera system was also developed to provide necessary synergism between SIR evaluation of an inspection zone and visual inspection. The resulting combination of technologies allows both evaluations to be performed without sacrificing location accuracy.

An SIR implementation tool was developed. The team fully recognized that SIR technology is not familiar to many engineers in the NDT community, so a flowchart and software module were developed to assist the practitioner in first determining if SIR can be used for a specific component. Assuming SIR is applicable, the software then provides guidance on how to address the necessary

SIR inspection variables. The software module is not considered complete at this point, but it will be tested with as many NDT professionals as possible to gain feedback for refinements.

The conclusions and recommendation from this research may be summarized as follows: (1) viable, inexpensive options for insertion of ADs for SIR testing were developed and demonstrated; (2) a DRA was developed and demonstrated to be a practical, versatile tool for realistic inspection scenarios. It is anticipated that the consistency afforded by implementation of the DRA will lead to improved NDT reliability estimates and a standard basis for rejection. Furthermore, the DRA will allow inspectors to focus on specific areas of interest, thereby reducing inspection time and the tedious nature of inspection; (3) a hybrid camera system was developed to improve synergism between SIR testing and visual verification of defects; (4) a prototype SIR implementation tool was developed for review by the customers and NDT practitioners to enhance implementation of the process in a production environment; and (5) the overall recommendation is to move forward with selected, specific aspects of the SIR technology to make disk inspection a practical reality.

1. INTRODUCTION

The primary objectives of this project for the sonic infrared (SIR) nondestructive evaluation (NDE) technology were (1) to advance development of artificial defects (ADs) for SIR, (2) to develop a computer-aided diagnostic and inspection tool to provide consistency of the SIR technique, and (3) to develop a set of rules for the application of SIR that will assist industry partners in determining which inspection tasks may benefit the most from the application of the SIR technique. In addition, a hybrid camera (visible and infrared) was developed under the contract.

SIR testing has its basic physical advantages and disadvantages, just like every other NDE technology. Eddy current inspection is limited by variable geometry and false calls from minor contamination. Fluorescent penetrant inspection is limited by the complex physics that would cause the fluorescent dye to penetrate the inspection surface, be drawn out, and then be detected by a manual process. A basic requirement for SIR testing is for all critical surfaces of the inspection subject to be excited sufficiently by a source (often an ultrasonic welding device) to allow defects of concern to emit enough heat to consistently be detected by a high-end IR camera system. Furthermore, the emission of heat must be in the line of sight of the camera or an assisting mirror that carries the image to the camera. There are special challenges for SIR testing of engine disks that are not particularly difficult for other flight engine components, such as blades. For example, disks are generally much more massive than blades from the same engine. Though a blade can generally be interrogated with an airfoil and root scan, disks require multiple excitations in various locations simply to assure activation of all critical areas and then provide adequate camera coverage to a sufficient sensitivity. At this point, it is not entirely clear how many excitations and what energy levels must be used to sufficiently excite a massive bore region, particularly when residual compressive stress is considered. Line of sight is a special consideration for disks. To conduct adequate inspection of multiple blade slots, many views may be required for adequate camera coverage, even when mirrors are implemented. Another consideration is coupling material and support points for disks. In the laboratory, simple business card stock is often used to isolate the inspection subject from the excitation source. For blades, special pinch blocks have been designed that eliminate the need for a coupling medium. No similar, practical device has been developed for disks. It is relatively straightforward to insert real fatigue cracks into small parts, such as blades. However, laboratory cracking of critical locations on disks is difficult, time consuming, and expensive. For these reasons, depot implementation of SIR testing for disks will lag behind implementation for most blades. A succession of technical programs can be formulated by a logical technical “roadmap” that recognizes the various special challenges and provides the means to overcome each major hurdle in the least amount of time with the lowest associated cost.

1.1 AD DEVELOPMENT

The goal of the AD task was to develop a method for the cost-effective fabrication of ADs on parts to enable the evaluation of the technique for applications in which relevant flaws are not readily available. These ADs should display similar spatial and temporal response to acoustic energization as fatigue crack defects to be used in the inspection process. The goal of this task will be to create a defect for SIR that is analogous to an electrical discharge machining (EDM) defect used for capability determination of eddy current tests. The details of AD development are found in section 2.

1.2 DEFECT RECOGNITION DEVELOPMENT

The goal of a defect recognition algorithm (DRA) is to assist operators analyzing SIR inspection data in determining if a relevant indication is present on a component. Relevant indications of interest in SIR inspection are primarily cracks occurring on the surface of the part. The DRA also aims to make the inspection analysis more reliable because human interpretation and human error are factors that affect reliability. The DRA is intended to make the decision process easier and clearer for the operator (is there a relevant indication present: yes or no?). With the existing SIR equipment, operators have several tools to use when analyzing the inspection results: raw data analysis, background subtracted analysis, max signal analysis, and pulse phase analysis. The initial intent of the DRA is to augment these tools, but the end goal is that with continued development, it will be the go-to method for crack indication detection. In its current state, the DRA is a useful tool that clearly presents the users with a color contour image showing where the relevant indications are located. The details of the DRA are described in section 3.

1.3 SIR IMPLEMENTATION TOOL

The goal of the SIR implementation tools (flowchart and software tool) are to guide users to a set of parameters suitable for their new component. With this set of recommended parameters, an optimization study can be conducted to fine-tune the parameters and fixtures of the inspection for that component. A flowchart and software package were created to provide a simple, easy-to-use experience and reveal the recommended parameters via flowchart results or report generation from the software tool.

1.4 HYBRID CAMERA CONCEPT

The goal of the hybrid camera concept is to improve the documentation and image data in SIR. This hybrid camera acquires IR and visual data from the same perspective to form a single hybrid image. The single hybrid image is comprised of an underlay image of the component and an overlay of defects (identified by the DRA). This image makes it easier for the users to locate and evaluate potential relevant defects.

System design and much of the basis for the experimental effort followed from work performed by Siemens Energy on an earlier FAA contract [1]. Siemens was the first organization to produce a viable SIR testing system that has been used on a regular basis in an engine depot environment. Though Siemens does not produce aviation engines, much of the technology has been applicable, and the authors are grateful to Siemens engineers for their willingness to assist when requested.

1.5 SIR EQUIPMENT

The following list describes the equipment of the SIR system:

- Branson 2000Xae Ultrasonic Welder
- FLIR A6700sc Mid-wave infrared (MWIR) camera
- Genie™ TS-C2500 Visible Camera
- NI USB-6525 for Branson I/O Triggering
- Winford DB44HD Breakout Board for Branson I/O Access
- 8-port Power over Ethernet Switch Hub for camera communication and visible camera power
- Computer

2. AD DEVELOPMENT

2.1 INTRODUCTION OF AD DEVELOPMENT

The goal of the AD task was to develop a method for the cost-effective fabrication of ADs on parts to enable the evaluation of the technique for applications in which relevant flaws are not readily available. These ADs should display similar spatial and temporal responses to acoustic energization as fatigue crack defects to be used in the inspection process. The following sections detail the process of design, selection, testing, results, and implementation of ADs.

2.2 DESIGN OF DEFECT SPECIMEN DISKS

The defect specimen disks were the platform for testing the performance of ADs under a SIR inspection. The disks were designed to be simple in geometry (flat and round) with an attempt to mimic behavior of a real engine disk. The round shape of the specimens mimics real disks better than square flat plates because the geometry of a component is a key driver in the mode shapes. AD features (such as through holes, tapped holes, EDM slots, etc.) were machined into the disk; the actual ADs (pins, set screws, and epoxy) were then inserted into the AD cavity features. This section aims to describe the design process of the defect specimen disks.

2.2.1 Selection of Disk Materials

Before the design of the disk geometry was determined, a selection process of suitable materials was performed. The desire was to find and manufacture two defect specimen disks from materials that best represent engine disk hardware in the field. The titanium alloy, Ti-6Al-4V, was selected because of its wide use as a turbine engine fan disk material. Similarly, the IN718 nickel alloy was selected for its wide use as a high-temperature disk alloy in the rear section of the compressors and turbines. The requirements to energize disks made of these alloys can vary because of their significant differences in material density, modulus, and inherent damping properties.

2.2.2 Design of Defect Specimen Disk Geometry

The defect specimen disks were the platform for testing ADs. It was desirable to keep the geometry of the disk simple to reduce manufacturing costs and remain practical (i.e., user friendly) from an

inspection standpoint. Sandia National Labs provided Florida Turbine Technologies (FTT) with retired disk hardware for this contract. The diameters of the disks ranged from 6–18″. It was decided that a diameter of 11″ would suffice for the defect specimen disk because it captured the approximate average size of the program's candidate disks. The thickness of the defect specimen disks was set to 1/4″. The thickness was determined by material costs and the feasibility of manufacturing AD features into the component. The inner diameter was sized to easily mount on the current fixture designs for a Honeywell auxiliary power unit (APU) candidate disk from Sandia. This allows the defect specimen disks to be mounted with the same hardware; therefore, the boundary conditions are consistent with an APU SIR inspection.

The location and positioning of the AD features were carefully considered. A layout was designed of the AD features such that they all lay in one quadrant of the disk. The features were separated circumferentially, 15º apart, with approximately 1.5″–2″ spacing radially. Having the features located in one quadrant provides flexibility with SIR excitation locations and provides sufficient room for future feature iterations, if desired.

Figure 1 shows all the key design and layout details of the defect specimen disk.

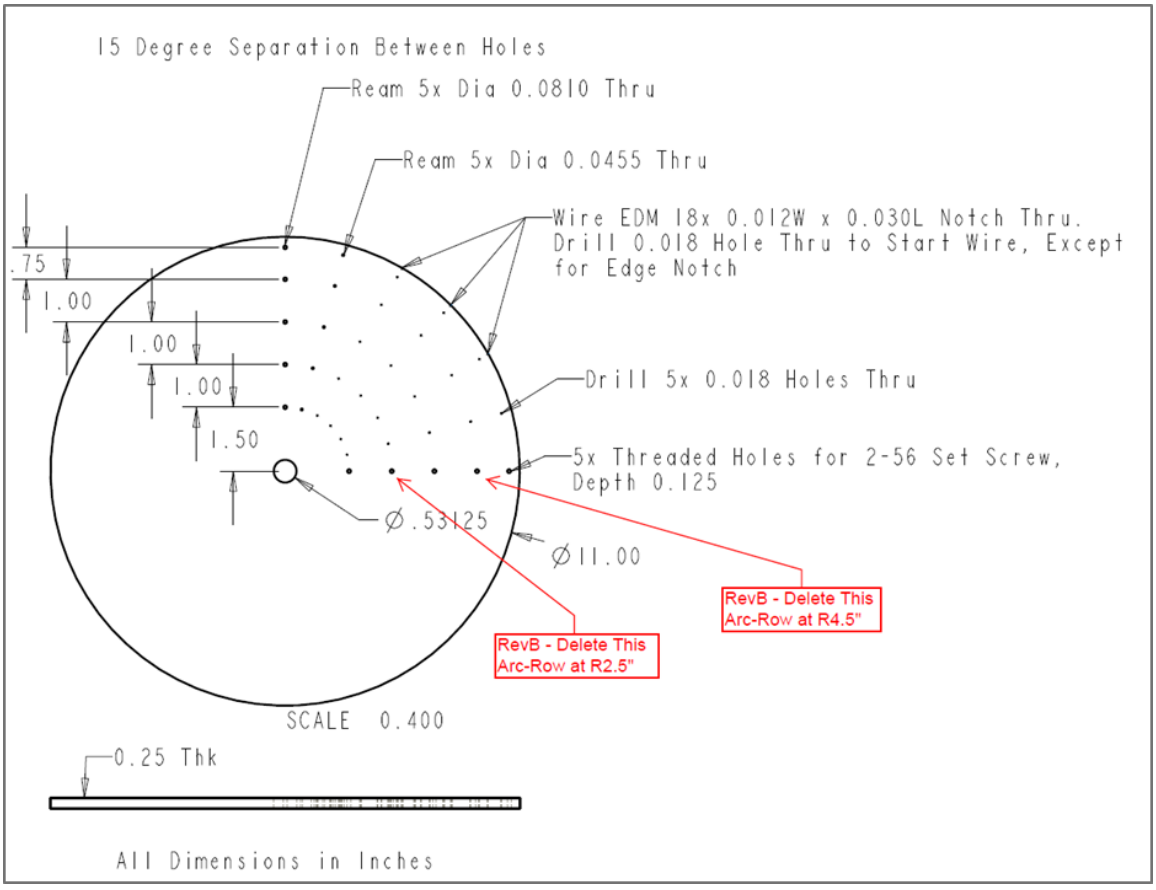

Figure 1. Defect specimen disk drawing

2.2.3 Fabrication Techniques of Specimen Disks and AD Features

The following describes the fabrication process for creating geometries and features in the defect specimen disk (see figure 1):

- Defect Disk Outer Diameter—Wire EDM cut from 1/4″ plate stock (IN718 and Ti6-4), 11″ diameter
- Defect Disk Inner Diameter—1/2″ drilled hole
- Press-Fit Pin Holes—Drilled and reamed to precision (0.081″ and 0.0455″ diameters)
- EDM Slots—0.018″ starter hole created by plunge EDM, then 0.030″ length slot was created with wire EDM process
- Set Screws—Hole plunged EDM to depth 0.125″, then tapped with 2-56 thread
- Through-Holes—0.018″ diameter plunged EDM through plate thickness

2.3 SELECTION, INSTALLATION, AND TESTING OF ADs IN SPECIMEN DISKS

2.3.1 AD Materials

The purpose of testing and developing a set of ADs comes from the desire to assess the viability of SIR inspections for components that do not readily have cracks. It would be ideal to assess the feasibility of SIR (for a given component) with a known crack, but such hardware is often difficult to obtain. ADs are an important resource because they can produce thermal signals similar to cracks and should be easily installed at multiple locations on a component. Ideally, a real crack would be desired when testing and tuning an inspection for a component. However, the fixtures, modal analysis, and labor involved in the cracking process can be costly. ADs provide an economical alternative to HCF or LCF crack production in a component.

FTT has experience with AD development under contracts with the United States Air Force (USAF) (FA8650-10-D-5210) for SIR of turbine and compressor blades. Under that contract, EDM notches, epoxies (various mixes), and press-fit pins (various sizes and tolerances) were assessed. This program built off the knowledge gained from that program. Four ADs were selected—0.046 and 0.082 press-fit pins, silver-filled epoxy (TiGA), and 2-56 set screws. The sizes of the defects were selected such that the defects were physically small (to provide surface contact areas on the order of crack sizes), yet remain within the limits of manufacturing. Press-fit pins and the epoxy have proven to be viable choices based on their performances on a previous contract (which tested multiple epoxy fillers and pin sizes and tolerances). Note that the epoxy is filled into EDM slots. Set screws have required features that are easy to manufacture, easy to install, and theoretically provide the surface-to-surface interaction that is similar to crack faces rubbing together to generate heat.

The AD materials that were selected are shown in figure 2.

Figure 2. AD materials

2.3.2 Defect Specimen Disks With ADs Installed

The defect specimen disks are the platform by which the ADs were tested. The defect specimen disks were manufactured to be simple, thin, round plates. Two identical disks were made—one made of Ti6-4 and the other IN718. See figure 3 for a view of the two defect specimen disks. Having two different materials allowed FTT to assess the performance differences between ADs due to material. The ADs were also compared among each other for the same material (section 2.3.3 details those results).

Figure 3. Defect specimen disks—Ti6-4 (left) and IN718 (right)

2.3.2.1 Installation process for each AD

The following was the installation process for the ADs:

- Set screw—Using a 0.035″ hex wrench, the 2-56 set screws were threaded in until hand tight. Then, using a torque wrench, the set screws were torqued to 2.5 in-lbs.
- Press-fit pins—A chamfer was created on the pin to help guide the pin through the reamed hole (with an interference of 0.001″). A press machine was used to force the pin all the way through the interference hole. A custom-cut collar was then placed around the pin, while pressing through, to keep the pin from buckling or moving off axis.
- Epoxy—The epoxy packets were mixed as prescribed. The EDM holes were filled with epoxy with a vacuum pulled on the opposite side of the hole to draw the epoxy through. The epoxy was cured as prescribed.

2.3.3 Experiments and Results of AD Materials in Defect Specimen Disks

The first trial of SIR AD experiments in the titanium and nickel disks were: 2-56 set screws, 0.046″ press fit pins, and 0.082″ press fit pins. There was a long lead time for the epoxy, so it was evaluated later (epoxy results are detailed later in this section). See figure 4 for a close-up view of the ADs. The disks were inspected with the SIR technique and the horn excitation locations were varied from (1) the outer radius–5″, (2) the mid radius–3″, (3) through the center of the disk/fixture. Ultimately, location (2) provided the highest energy response, so that horn location was used for the data shown in this section. See figure 5 for an illustration of excitation locations. Card stock was used as the interface layer—the same interface layer used during SIR of the JT8D. A set of inspections was conducted that varied the horn excitation location, but held all other control parameters similarly (roughly equivalent parameters for inspecting JT8D—0.7sec excitation, 10

psi, 80% amplitude). This would allow FTT to investigate the performance/response/signal of the different AD types based on varying horn locations.

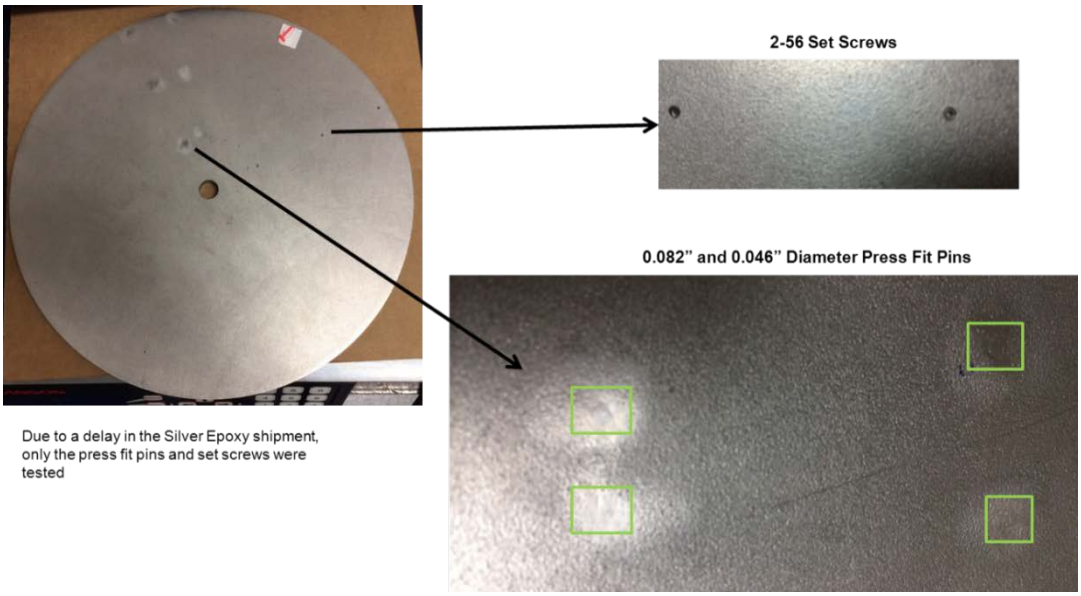

Figure 4. ADs installed; set screws and press fit pins

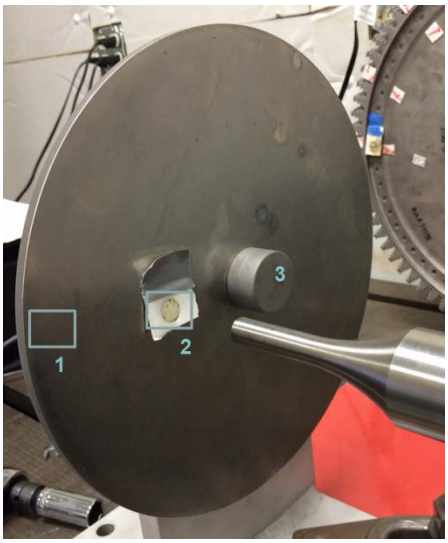

Figure 5. Excitation locations of AD disk for SIR

Ultimately, location (2) provided the highest energy response so that the horn location was used for the data shown in this section. Location (1) resulted in frequent ultrasonic power supply overload conditions, thereby making that location undesirable. Location (3) did not provide sufficient energy into the component, thereby making that location adverse for SIR testing. Examples of post-processed SIR inspection data are shown in figures 6 and 7. These data were very encouraging because the ADs appear to behave similarly to real defects—their heating/cooling profiles are similar, especially for the IN718 disk. Figure 8 is an example of a real crack's SIR signal in a JT8D disk. Note that the data in figure 8 used a simple average algorithm,

meaning that the pixel's plotted data was the average of itself with its neighboring pixels (8 x 8 region).

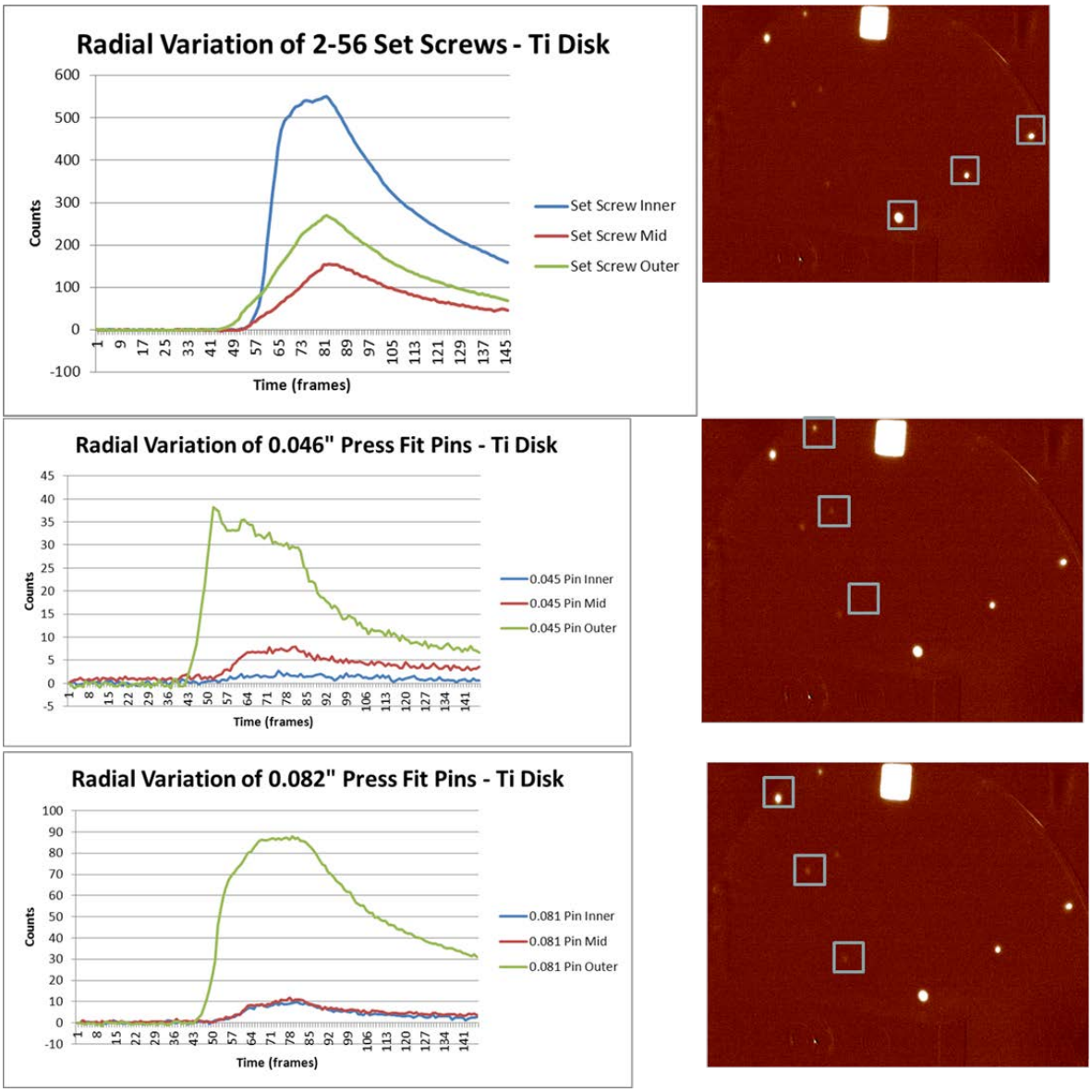

Figure 6. Radial variation of ADs in Ti disk

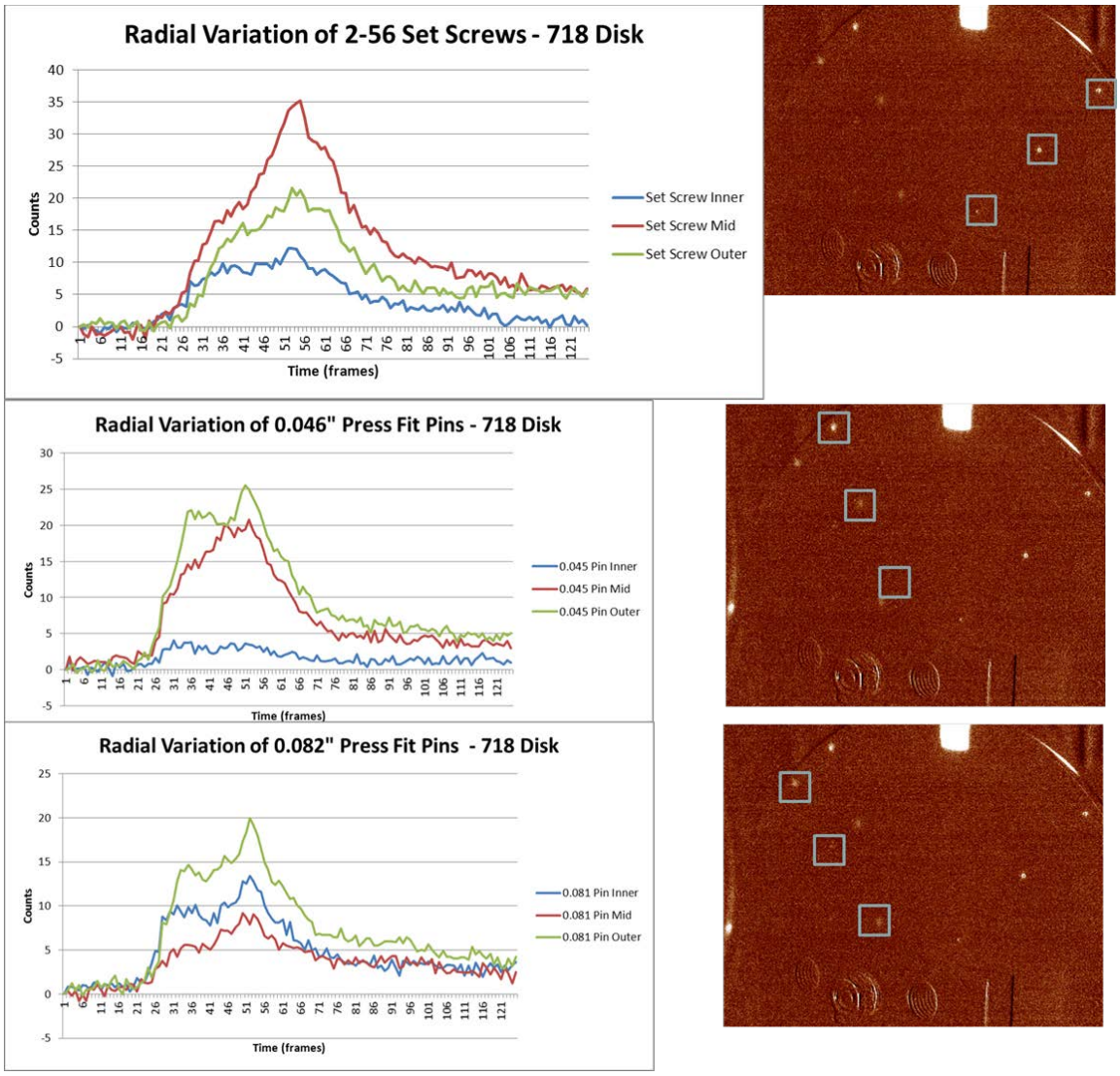

Figure 7. Radial variation of ADs in IN718 disk

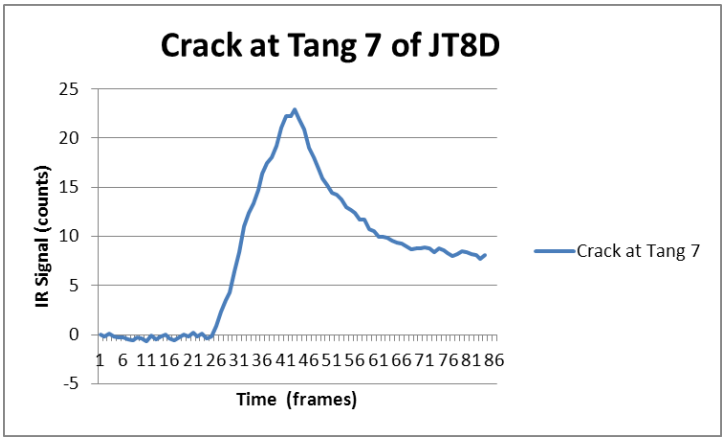

Figure 8. Example of SIR signal from a crack in JT8D disk, simple average algorithm

Approximately 1 month after the previously detailed investigation, FTT installed the TiGA epoxy in the EDM slots that were machined into the AD test disks. Figure 9 shows the epoxy locations before they were sanded down flush to the surface.

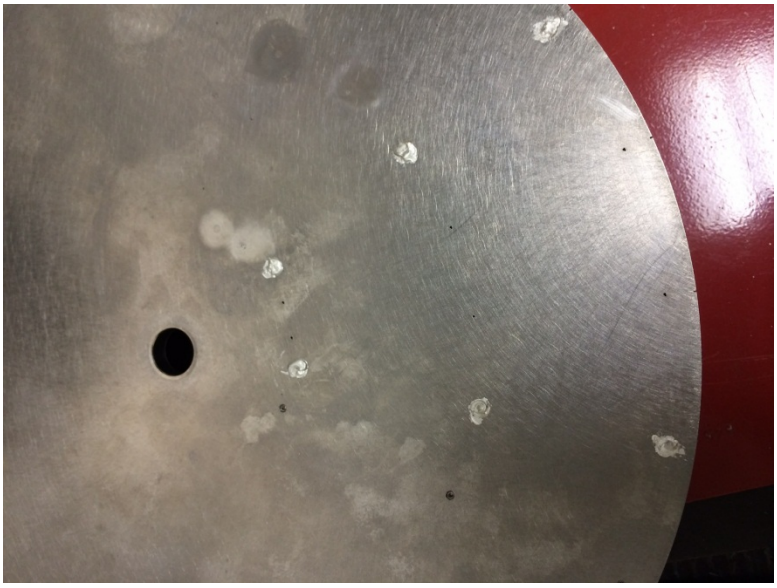

Figure 9. Epoxy installation on test disk, pre-sanding

After the epoxy cured, the disks were reinspected with SIR to understand the response characteristics of the epoxy AD. The data were then post-processed by an ImageJ algorithm developed by FTT. The algorithm inspects user-defined regions of interest (ROI) and finds the maximum signal from an averaging of an 8 x 8 region around each pixel in the ROI. In the previous experiment (without the epoxy AD), FTT illustrated the thermal response using only a simple average within an ROI.

FTT wanted to investigate the remaining AD epoxy. For reference, the IN718 disk was inspected with the following settings: 80% amplitude, 0.70s, and 12 psi; the Ti6-4 disk was inspected with the following settings: 40% amplitude, 0.70s, and 12psi. The Ti6-4 has higher response characteristics than the IN718, so the amplitude was lowered to avoid overloading the Branson power supply.

Figures 10–13 reveal the thermal response of all the inspected ADs.

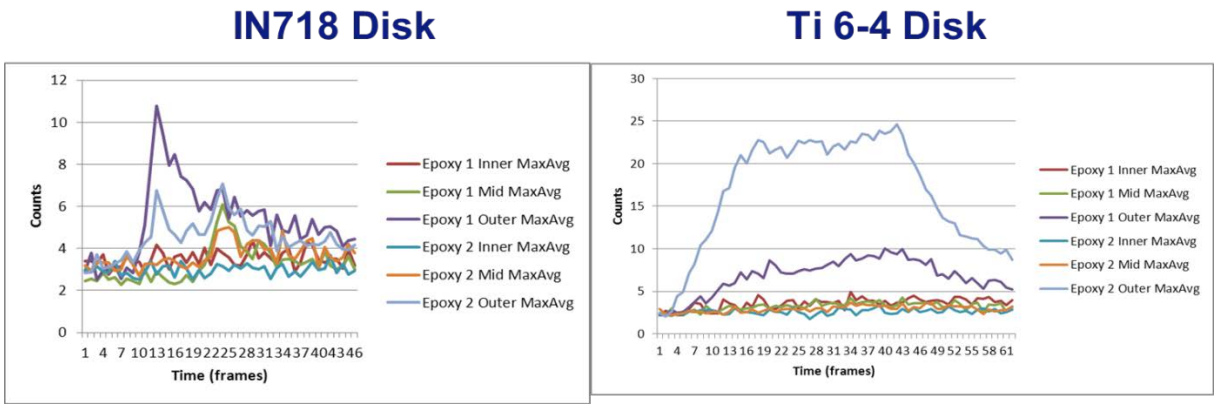

Figure 10. Epoxy, SIR response

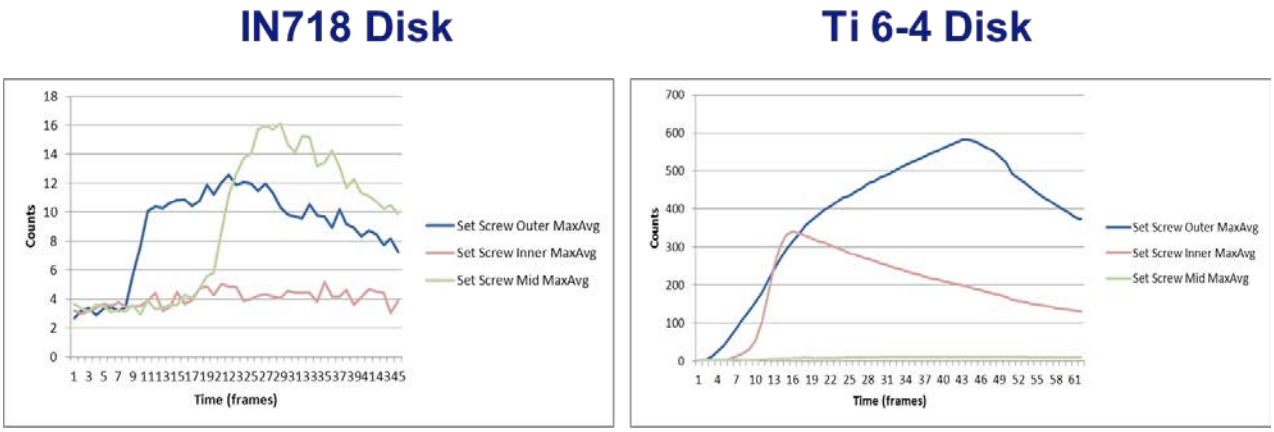

Figure 11. Set screws, SIR response

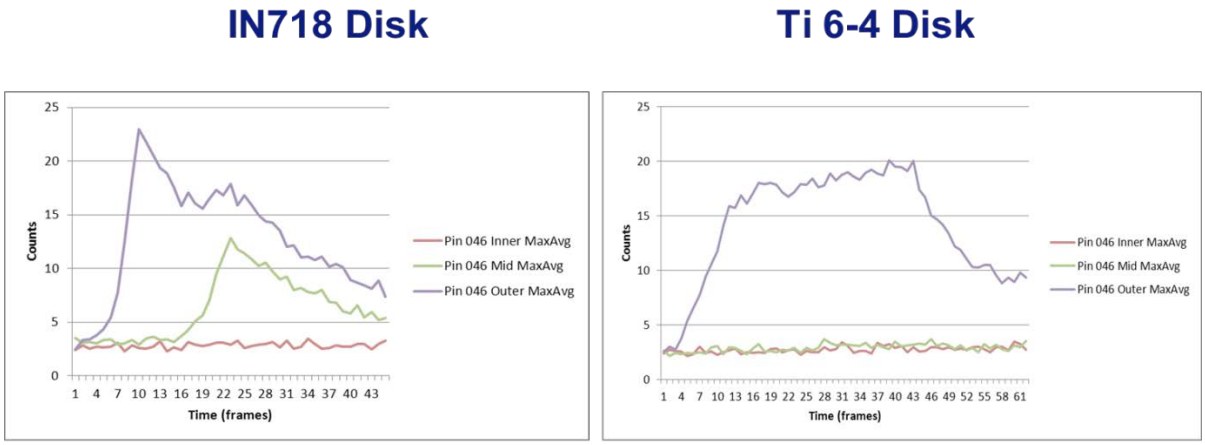

Figure 12. The 0.046 press-fit pin, SIR response

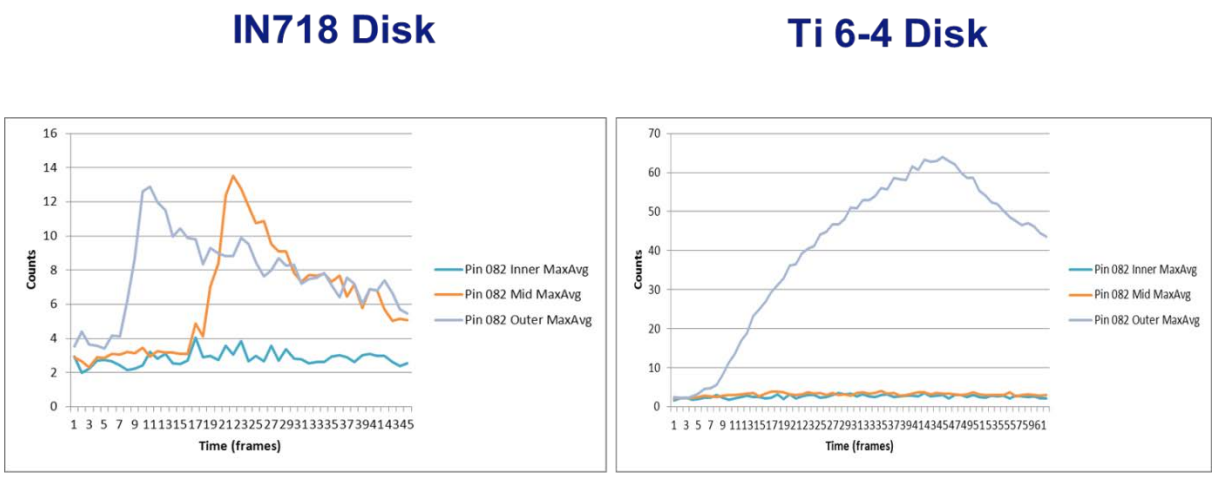

Figure 13. The 0.082 press-fit pin, SIR response

For reference, figure 14 is the thermal response from cracks in the JT8D disk, using the same max average 8 x 8 processing.

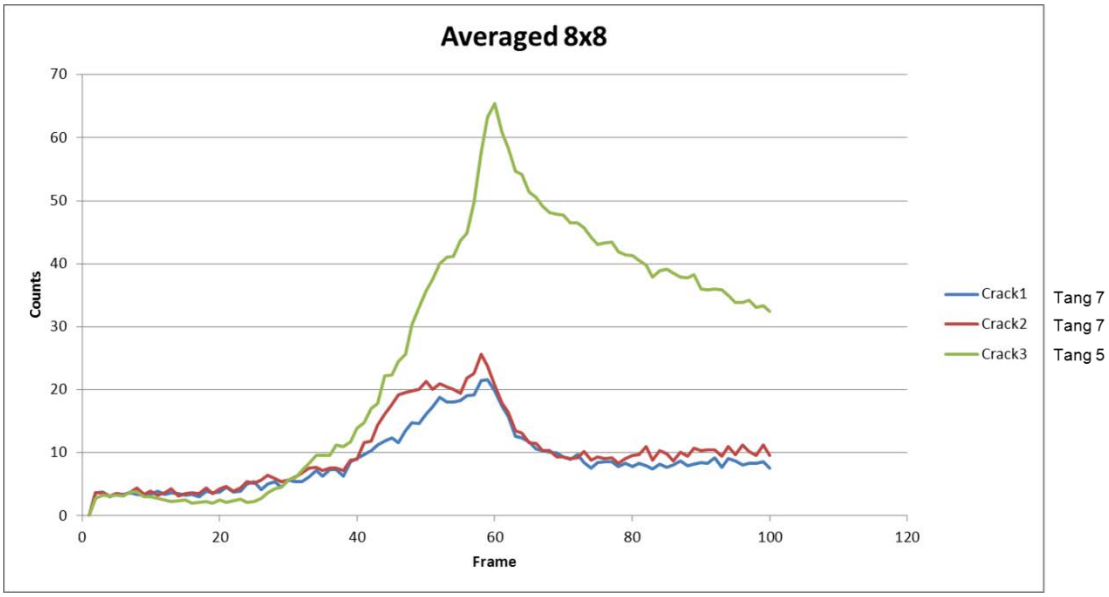

Figure 14. Example of SIR signal from a crack in the JT8D disk, max average 8 x 8 signal algorithm

2.4 SUMMARY OF AD MATERIAL EXPERIMENTS

The following is a summary of the AD material experiments:

- The press fit pins and set screws perform the best.
  - Their thermal signals are similar in behavior to real cracks.

  - Their thermal rise and decay, temporally, correlated well with crack thermal signals, and their peak amplitude was sufficiently above the noise floor.

- The epoxy has a lower amplitude response than desired.
  - Could be due to the small 0.030″ slot.
    - Not enough volume of epoxy.

In the USAF-sponsored SIR program, press fit pins out-performed the epoxy, so this may be no surprise.

- The differences in quality factor (Q factor) of the materials posed some challenges.
  - Note: Higher Q indicates a lower rate of energy loss relative to the energy dissipation of the excited resonances; the oscillations decay more slowly.
  - Titanium has a higher Q factor than nickel.
    - Parameters were appropriately adjusted to mitigate the risk of overloading the Branson power supply but still maintain a quality inspection.

As a result of the summary above, numerous 2-56 set screws were installed in the JT8D second-stage turbine disk to test the responses in an actual engine component. Set screws were selected over the press-fit pins because press-fit pins were being investigated as an airfoil AD under a concurrent USAF program (FA8650-10-D-5210). Details and results for the AD performance in the JT8D disk are detailed in the following sections.

2.5 MANUFACTURING OF SET SCREWS IN JT8D SECOND-STAGE TURBINE DISK

2.5.1 Design and Layout of Set Screw Locations for Manufacturing

FTT recommended that press-fit pins and set screws were the best AD candidates for testing in a real engine disk. Economically, it made sense to select one candidate to test in real hardware. Set screws were ultimately selected because of their simplicity of installation and manufacturing and their realistic thermal response. In addition, the press-fit pins were already being investigated as an AD under a concurrent USAF program on engine blades (FA8650-10-D-5210).

FTT conducted a design review internally and externally to the program team (FAA contract members and the like). After the locations and quantities of the ADs were solidified, FTT formally created the necessary manufacturing layouts. The following information was provided to the manufacturing shop for modifying the JT8D second-stage turbine disk:

- Features to be added include:
  - Drill and tap:
    - Six #2-56 threads into the forward (FWD) face of the disk at two clocking locations at various radial positions in line with existing fir trees featuring cracks
    - Two #2-56 threads into the FWD face of the disk at two clocking locations at two radial positions on fir trees with no cracks
    - One #2-56 thread into the FWD face of the disk at two clocking locations at the root between two adjacent fir trees
      - 18 total tapped FWD-end holes
    - Four (4) #2-56 tapped holes at two clocking locations at outermost 4 radial positions
      - eight total tapped AFT-end holes
    - One (1) #2-56 threads into center of the inner hub at two clocking locations
      - two total tapped, hub holes
    - 28 total drilled and tapped holes

Note that the set screws were placed from the inner bore, out radially through the web, into the rim, and at the fir tree. These locations provide full radial coverage for SIR analysis.

Positional and envelope information was provided to manufacturing via PowerPoint® diagrams. See figure 15 for an example of a diagram supplied to the manufacturing facility. Note that figure 15 shows the FWD side of the disk. Similar diagrams were provided for the AFT-side and bore areas. See appendix A for all figures supplied to the manufacturing facility.

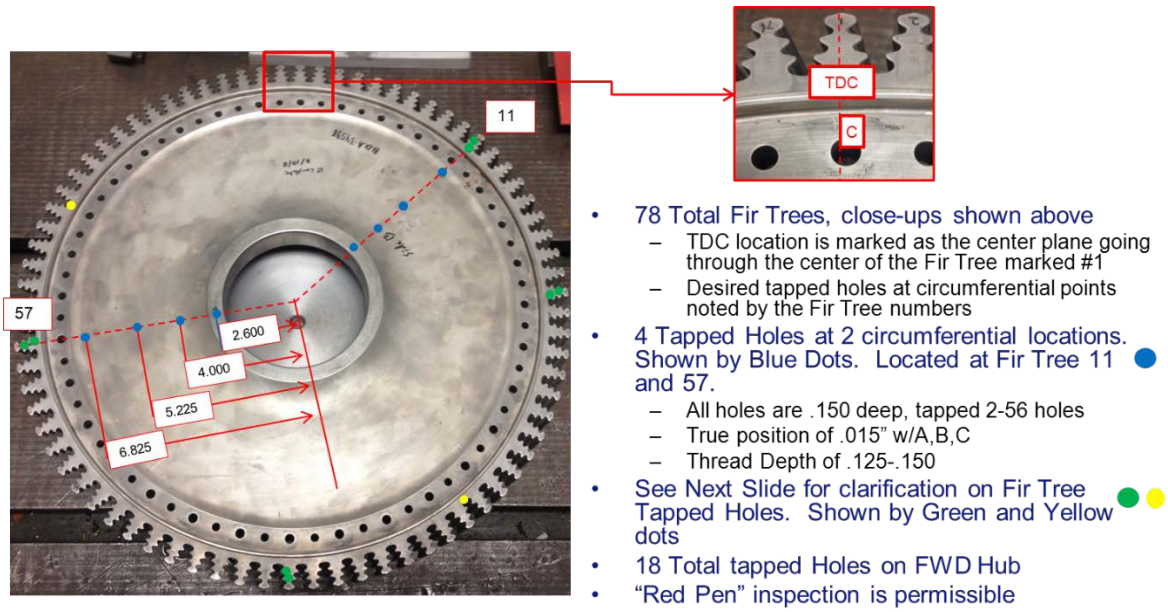

Figure 15. Example diagram detailing AD locations for manufacturing

2.5.2 Results of Manufacturing Set Screws in a JT8D Disk

Figure 16 reveals a few examples of set screw manufacturing results in the JT8D second-stage turbine disk. FTT verified and quality-checked the component's newly manufactured features. All the threaded holes were clean and a set screw could easily be installed and bottomed out.

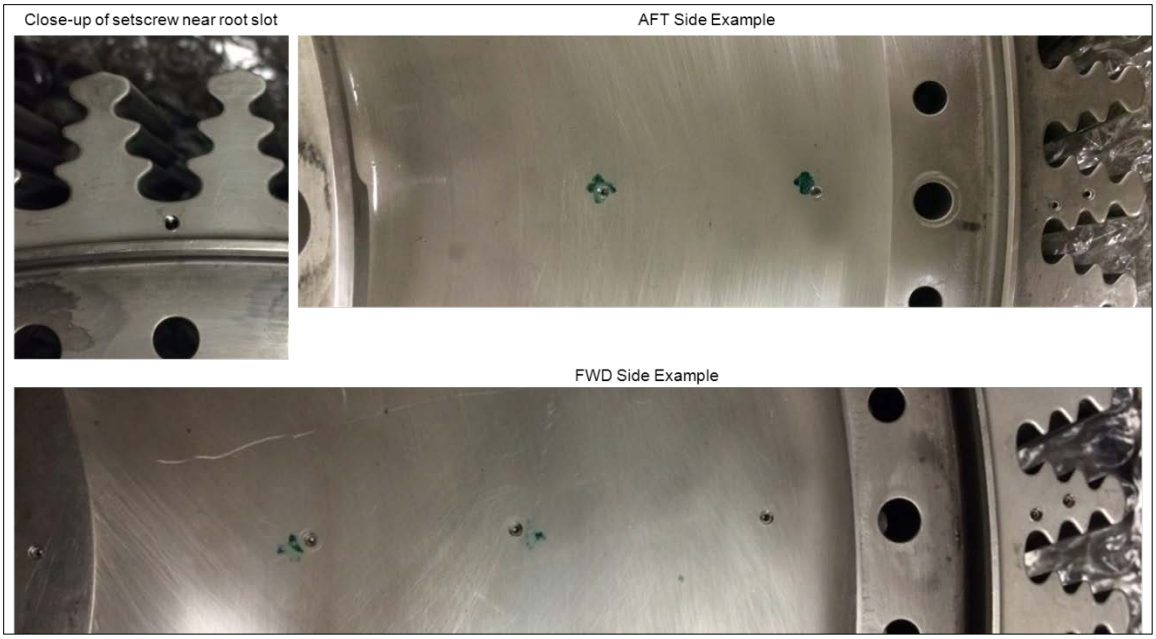

Figure 16. Close-up views of 2-56 tapped holes installed in JT8D second-stage turbine disk

2.6 THERMAL RESPONSE OF SET SCREWS IN JT8D DISK UNDER SIR INSPECTION

2.6.1 Inspection Parameters and Details

The settings for the Branson ultrasonic excitation source were 0.5 sec, 80% amplitude, and 12 psi (excitation time, signal amplitude, and contact force pressure, respectively). All plots in subsequent sections use the max-average calculation within an ROI around the AD. See figure 17 for an illustration of the horn contact location and card stock (coupling material) location. The card stock provides a sufficient transfer of energy while preventing metal-to-metal contact between the disk and the excitation horn.

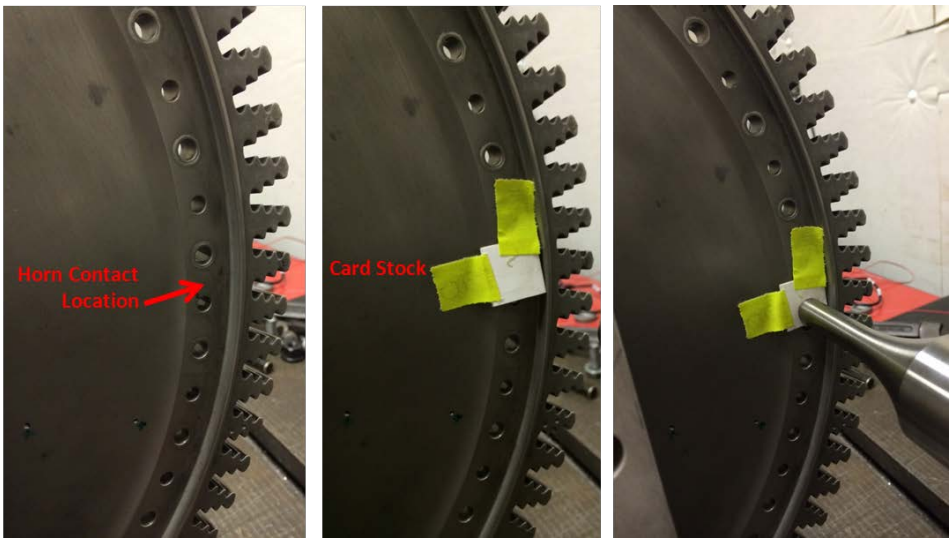

Figure 17. Horn contact location

2.6.2 General Results of Set Screws Under SIR

Twenty-eight set screws were installed into the JT8D disk. This section highlights one portion of the disk that has set screws installed at various radial locations on the disk. This was done to gain an understanding of the general trends of the set screw signals and any radial trends—particularly peak-amplitude trends.

Figure 18 shows the locations of the set screws and cracks in the field of view of the inspection. This figure shows that the set screws reveal themselves well against the background (in this scenario, the “background” is simply the disk face). Figure 19 shows the temporal responses of the set screws and cracks under an SIR inspection. In general, the peak amplitude decreases radially inward to the bore. This is expected since the excitation source is out near the rim, and the disk is fixed near the bore.

(a)

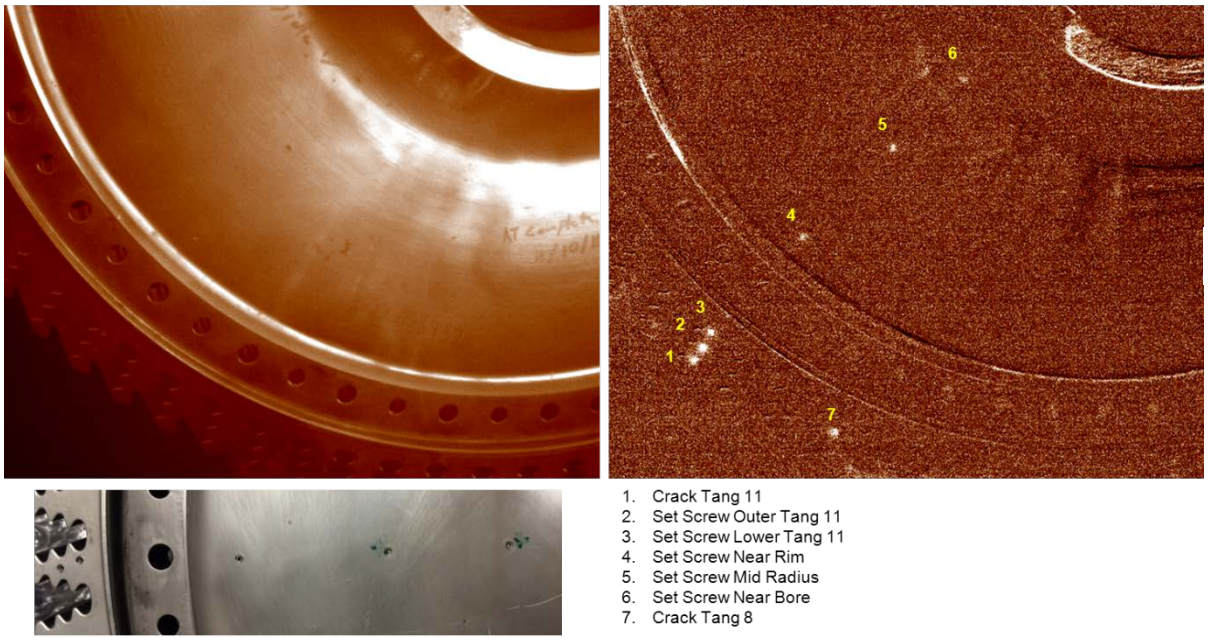

(b)

1. Crack Tang 11
2. Set Screw Outer Tang 11
3. Set Screw Lower Tang 11
4. Set Screw Near Rim
5. Set Screw Mid Radius
6. Set Screw Near Bore
7. Crack Tang 8

(c) (d)

Figure 18. An (a) IR View of JT8D disk near Tang 11, no processing; (b) background subtracted view of disk revealing set screw thermal results; (c) view of set screws with visible camera; and (d) list of features in background subtracted image

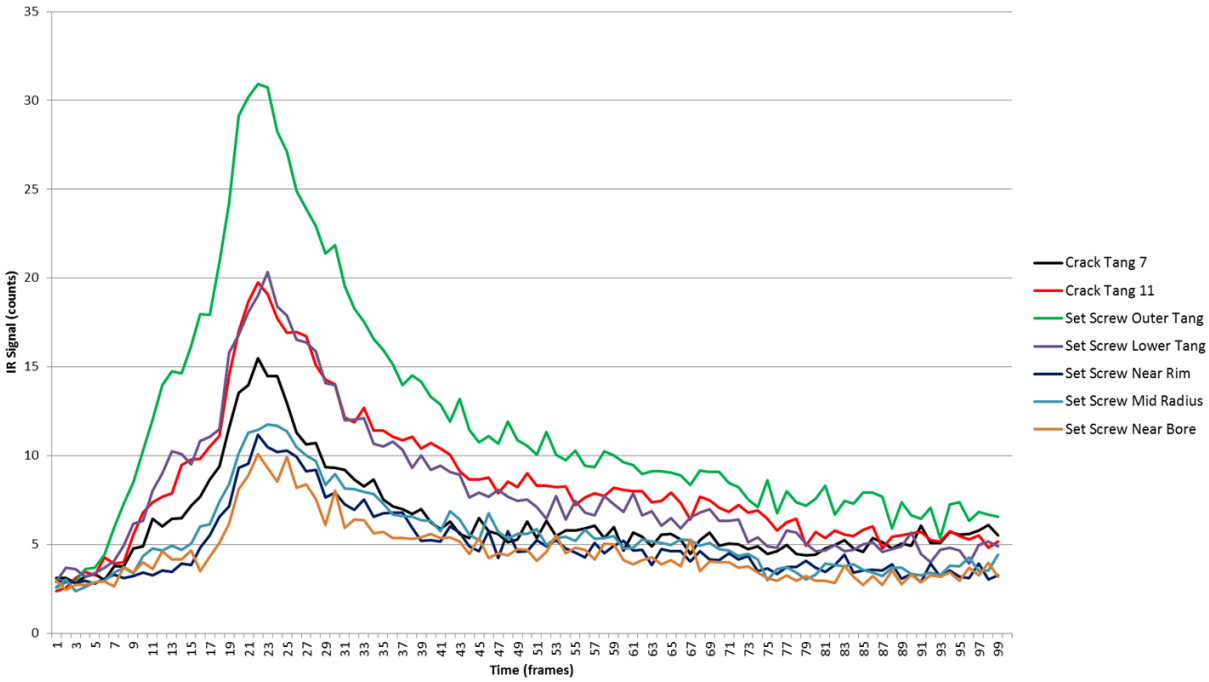

Figure 19. Thermal response of features (cracks and set screws) in JT8D disk

Conclusions from the data shown in figures 18 and 19:

- The IR responses from the set screws are similar to typical crack signals.
- The heating and cooling profiles of the set screws are well behaved and trend like in-service cracks in an actual turbine disk.

These results indicate that the set screw ADs, installed in the JT8D disk, produce crack-like thermal responses.

2.6.3 The Effect of Torqueing a Set Screw Below Surface

There was a desire to observe how torqueing the set screws down affected the thermal signal, as opposed to keeping the set screws untorqued and flush with the surface. Unfortunately, the manufacturing of the threaded holes and the length of the set screws were such that a torqued set screw was a couple of threads below the surface of the disk (not flush). Figures 20 and 21 show where the torqued versus untorqued data were recorded—near tang 31 of the disk.

(a)

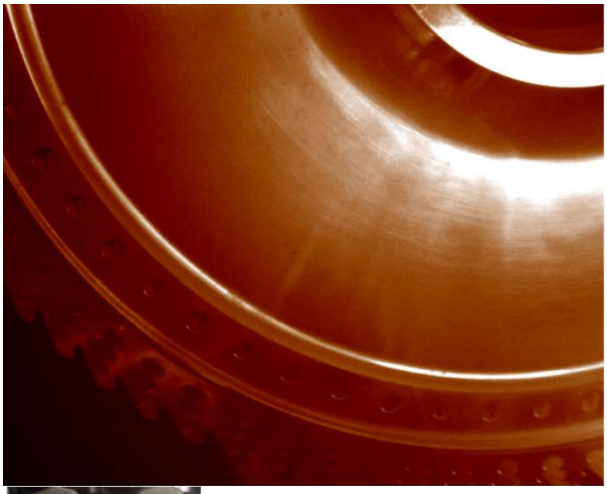

(b)

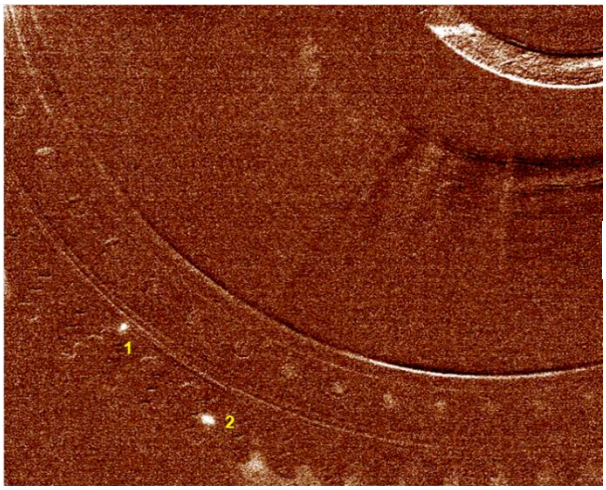

1. Set Screw in between Tang 31-32
2. Crack Tang 29

(c) (d)

Figure 20. An (a) IR view of JT8D disk near Tang 31, no processing; (b) background subtracted view of disk; (c) view of set screws with visible camera; and (d) list of features in background subtracted image

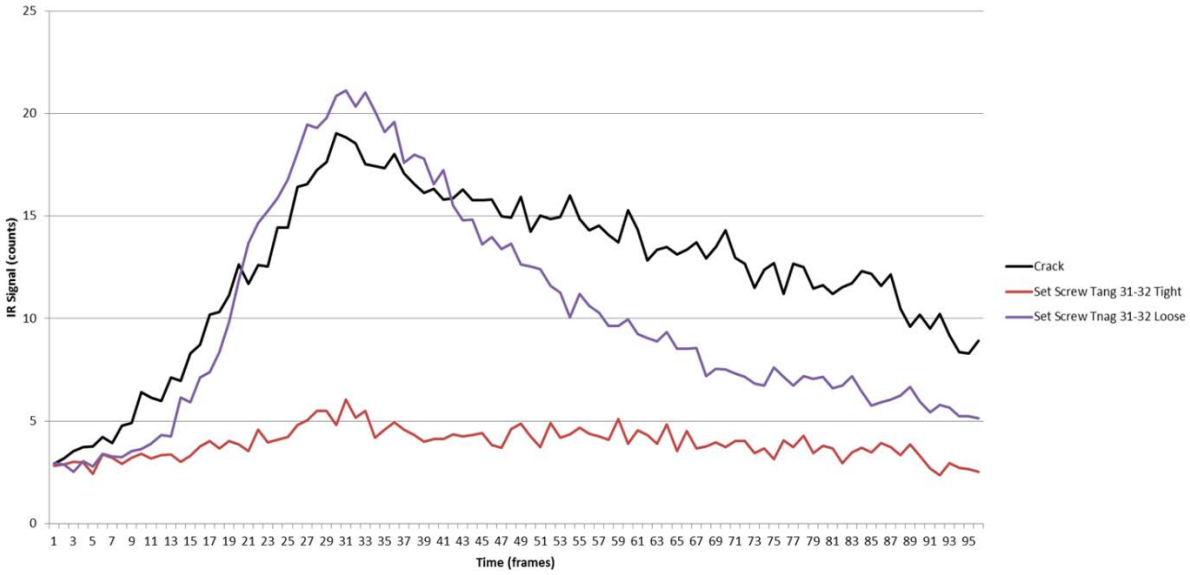

Figure 21. Thermal response of crack and set screw (torqued vs. untorqued)

These results were counter-intuitive, so a second study was conducted. There was concern that having the set screws torqued too far subsurface could impact the heat seen at the surface by the IR camera. The setup of the second AD study for disk bore inspection using untorqued set screws is shown in figure 22.

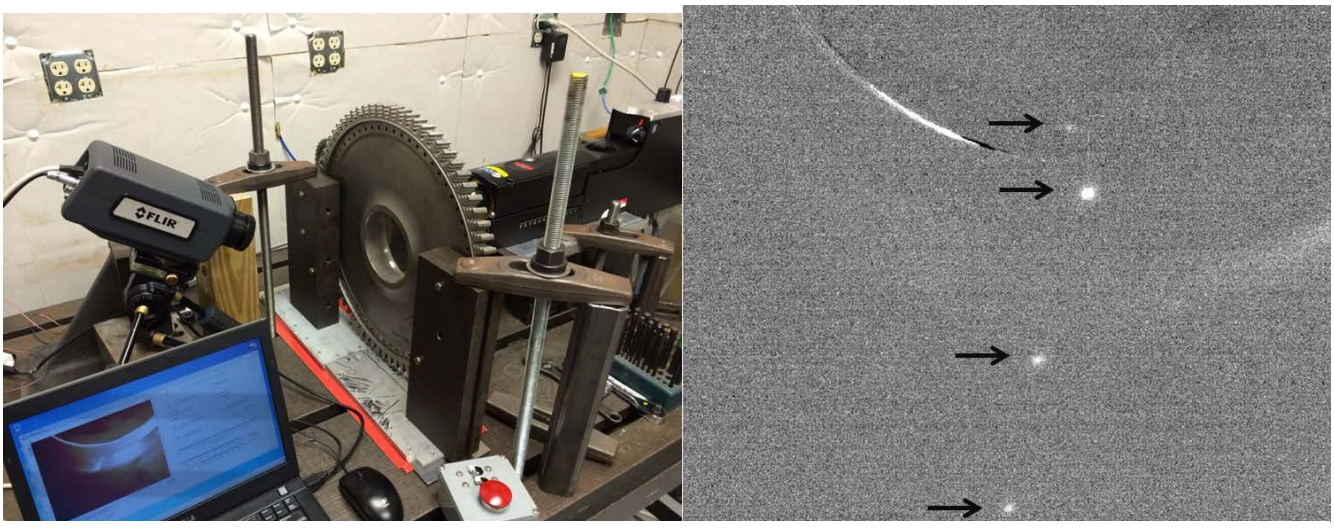

(a) (b)

Figure 22. The (a) bore inspection setup for SIR and (b) example results of SIR bore inspection

The set screws used in this case were installed nearly flush with the surface but left untorqued because of the concern that if subsurface and seated against the hole bottom, the set screws would dissipate heat too quickly for SIR detection. To test this theory, longer set screws were installed with the screw heads either flush or slightly raised above the bore surface. The following variants

were SIR inspected: 1) no set screw, 2) an untorqued set screw, and 3) a torqued set screw. This set of variants covers the scenarios of concern and helps one to understand the effects of torque and thermal response. The results show that, contrary to a previous trial with short set screws, the longer torqued set screws performed very well (in some scenarios, arguably better than untorqued—see figure 23).

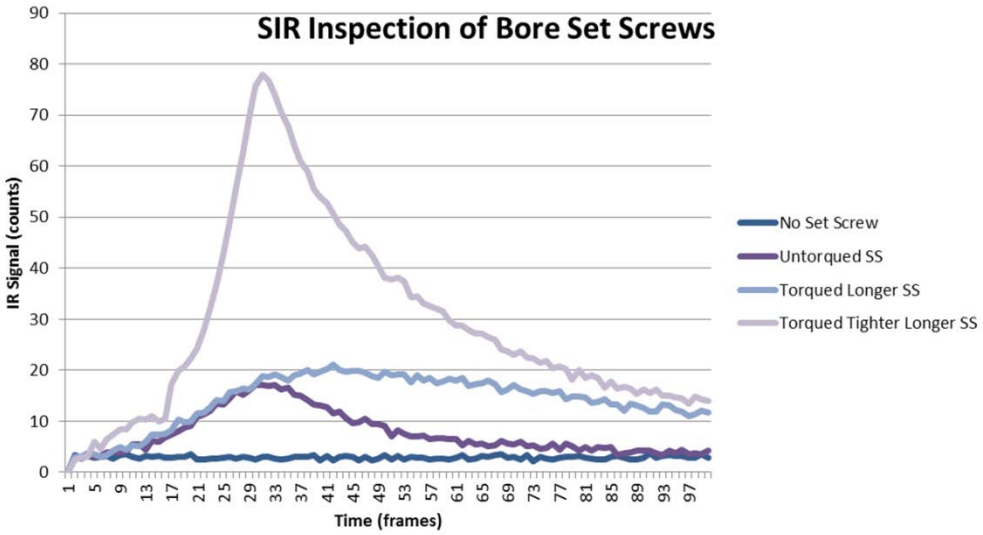

Figure 23. SIR results for set screws in bore: torqued, untorqued, and no set screw

These results lead to FTT re-conducting the same trial they performed earlier in the contract. Figure 24 shows the location of the previous trial; it is labeled “close to excitation source.” The team wondered if excitation location significantly affects the mode shape, thereby affecting the response characteristics of the set screws at different locations. Figure 25 shows the results for the set screws near the excitation location, for both torqued and untorqued scenarios. Figure 26 shows the results for the set screws away from the excitation location, for both torqued and untorqued scenarios.

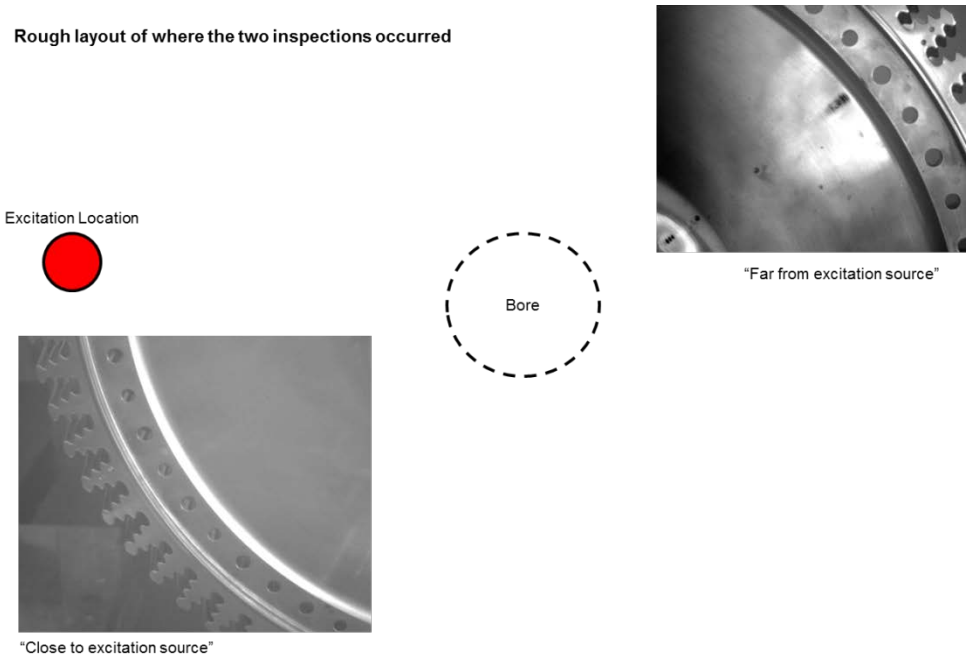

Figure 24. Layout of set screw and excitation locations for the retrial of torqued vs. untorqued set screws

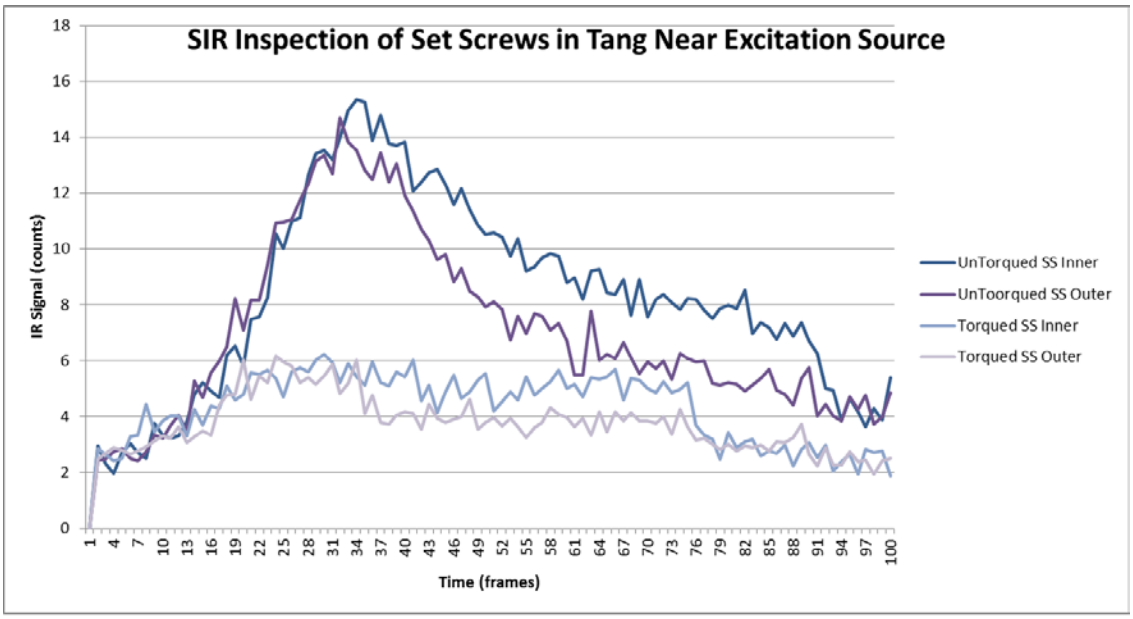

Torqued Set Screws produce poor results. This agrees with a trial conducted earlier in the contract.

Figure 25. SIR inspection results of set screws near excitation source

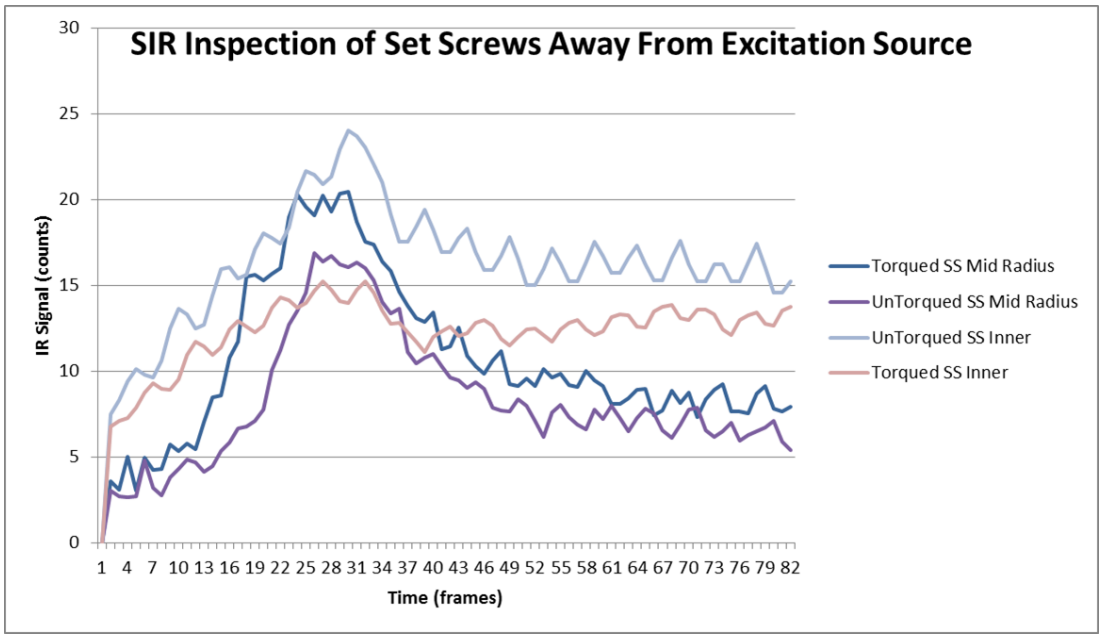

Figure 26. SIR inspection results of set screws away from excitation location

2.6.3.1 Conclusions Based on the Torqued vs. Untorqued Data

Conclusions and theories for the observed results:

- Why do the torqued set screws perform poorly when they are near the excitation source?
  - Mode shape(s) has reduced amplitude near excitation source.
    - Tap near the excitation spot to ring the disk; more amplitude/motion on tangs away from the tap zone.
- Why did the bore set screws work better torqued/untorqued even though they are close to the excitation source?
  - Fixture setup was completely different—promotes different mode shape(s).
- Torqued set screws are a viable AD option.
  - Lesson learned to consider the mode shape(s) as the mechanism that reduces amplitude, not simply the fact that it was torqued.

2.6.4 Small Sample Repeatability Study of Set Screw Thermal Responses

In the previous section, it was discovered that untorqued set screws (i.e., flush with the disk surface) produce better results than the torqued set screws (which get fastened 2–3 threads below the disk surface). A small sample repeatability study was conducted to observe the variations test-to-test of the untorqued set screws. Tang 40 of the JT8D disk (which contained two set screws in the tang) was used for this experiment. See figure 27 for an illustration of the AD locations and an IR view of their thermal response.

(a)

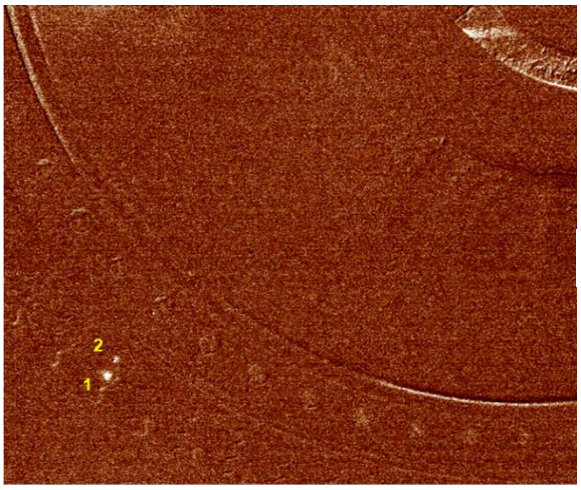

(b)

1. Set Screw Outer Tang 40
2. Set Screw Lower Tang 40

(c) (d)

Figure 27. An (a) IR View of the JT8D disk near Tang 40, no processing; (b) background subtracted view of the disk; (c) view of set screws with a visible camera; (d) list of features in background-subtracted image

The small sample repeatability study was comprised of 11 consecutive tests with 30–60 seconds of delay between tests. The excitation parameters were the same as the parameters detailed in section 2.6.1.

Figure 28 reveals a typical thermal response of the two set screws in Tang 40 when excited under an SIR inspection. Figures 29 and 30 show the temporal thermal responses of all 11 subsequent tests. Figure 31 shows the peak amplitudes from each test and provides statistics on data.

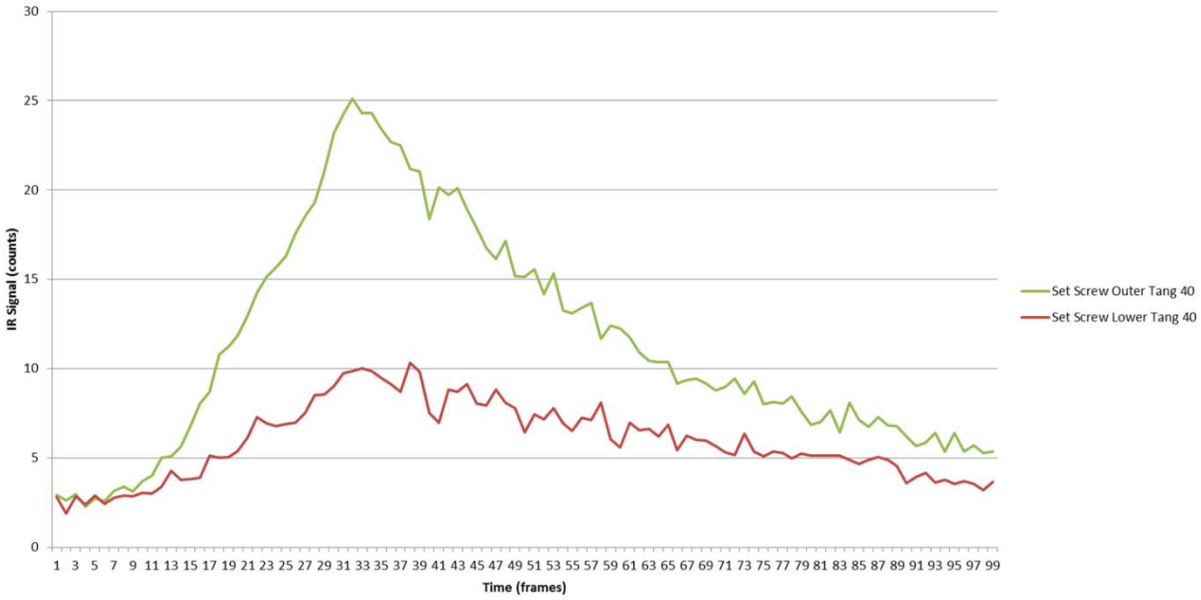

Figure 28. Example of the thermal response of set screws in Tang 40

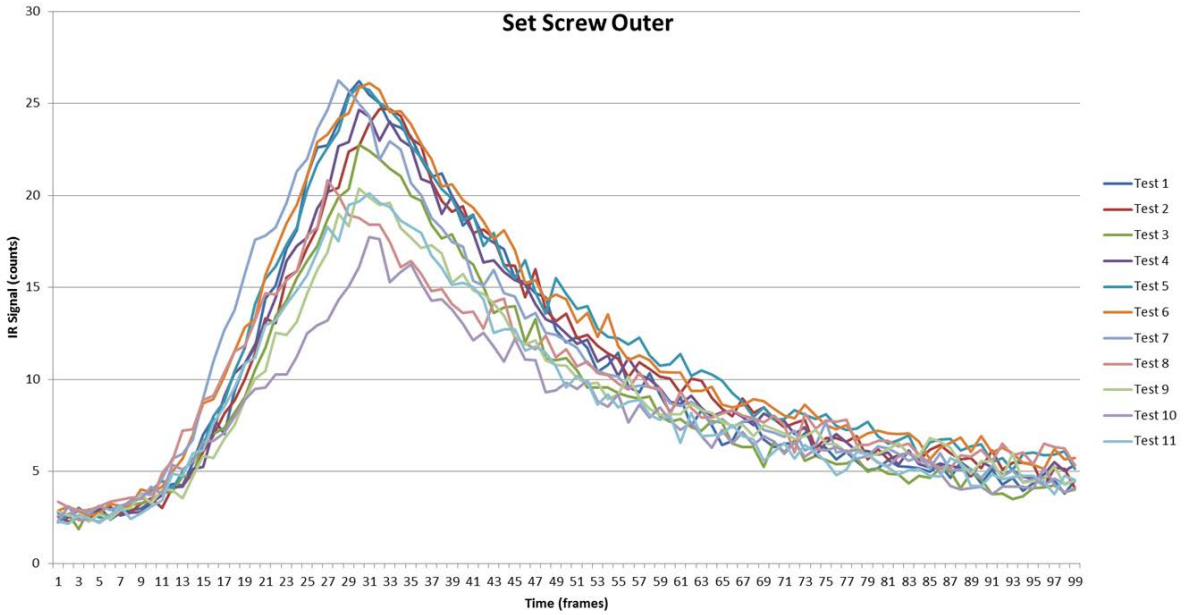

Figure 29. Thermal response of outer set screw in Tang 40, repeated tests

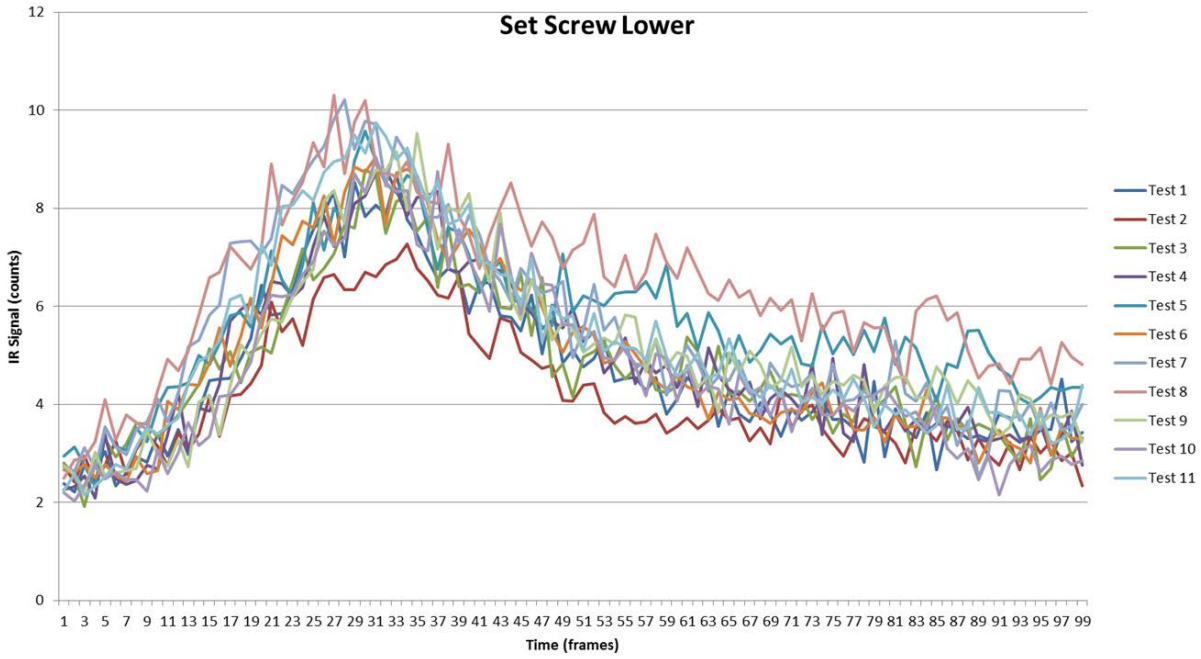

Figure 30. Thermal response of lower set screw in Tang 40, repeated tests

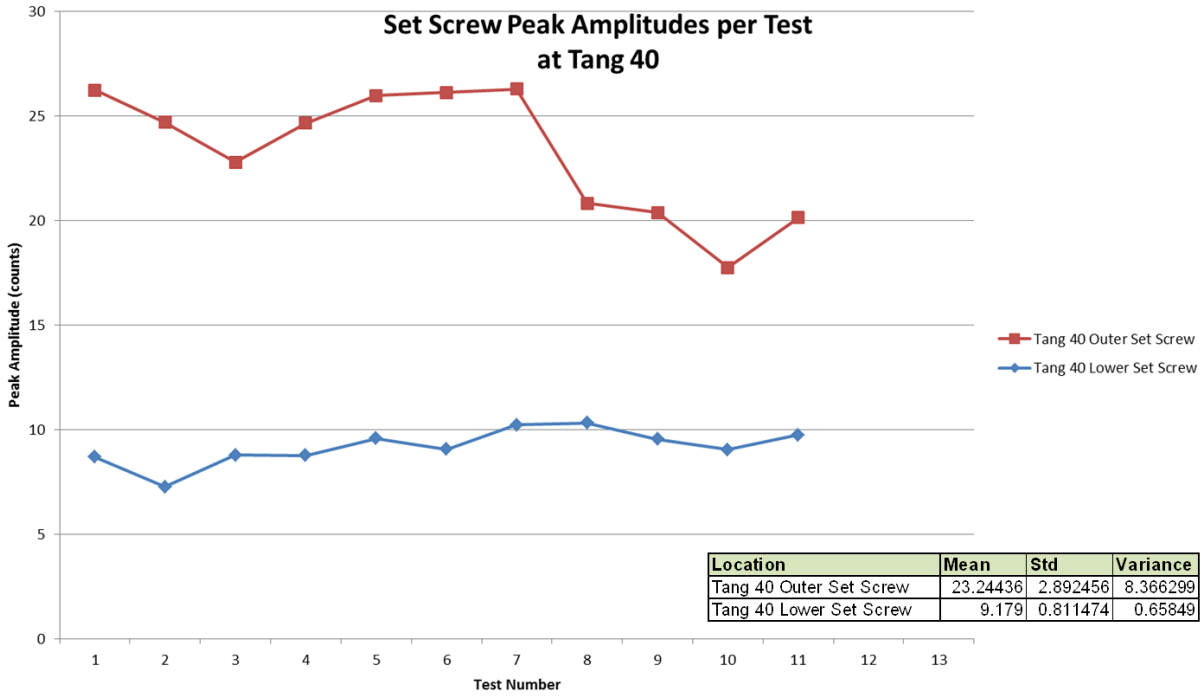

Figure 31. Peak amplitudes of set screw thermal responses and statistics at Tang 40

2.6.4.1 Observations Based on the Repeatability Data

The following are observations based on the repeatability data:

- Location affects the repeatability of the set screws.
  - This is not too surprising based on results from previous contract programs.
  - However, the ratio of standard deviation over the mean is approximately 10% for both.
  - Detectability was not compromised because the peak values were above the noise threshold, and the heating/cooling patterns were well-defined.
- Theories to explain the trends viewed in figure 31:
  - The outer set screw experiences more dynamic motion than the set screw that is closer to the rim.
    - Imagine that locally the tang is acting like a cantilever beam under excitation.
  - The dynamic motion is transient and not perfectly repeatable, so a few Joules difference in energy may affect the peak amplitude of the outer set screw.
    - This is characteristic of the chaotic excitation.

2.7 SUMMARY OF MANUFACTURING SET SCREW ADs IN JT8D DISK

The experiment of installing the set screw ADs into the JT8D second-stage turbine disk proved to be successful. The set screws were well-behaved and produced thermal signals similar to their crack counterparts. Set screws were selected because they produce quality heating/cooling profiles when excited under SIR, and they are economical from a manufacturing standpoint. The results of the data show that the set screws should be considered as a viable AD, especially for the scenario of determining capability or feasibility of the SIR method for components of which actual cracked parts are not available.

The following can be stated:

- The set screw ADs thermally behaved in a cracklike manner in the JT8D disk.
- Tightening the set screws below the surface of the disk reduced heat generation to the point at which it was difficult to detect any signal.
- Set screws that are flush with the surface produce heat that is easier to detect because the heat generation is at/near the surface.
- Repeatability appears to be location dependent.
  - Energy is not transmitted equally through the component; therefore, some areas are excited more than others simply because of the ultrasonic horn location.

- This is likely because of the multimode shapes.

- Set screws are viable and economical ADs for assessing inspection capability.

3. DRA DEVELOPMENT

3.1 SURVEY OF METHODS FOR SIGNAL PROCESSING

The research for DRA started with a survey of the signal-processing methods used in the industry. The first methods to be assessed were from the turbine online-monitoring technologies, which use prognostic and diagnostic methods for assessing the health of engine components. Pattern-recognition technologies were also investigated; these often involved learning algorithms and black box modeling techniques like neural networks and genetic algorithms. Filtering and signal reconstruction methods being developed by the academic community were also assessed, as were those used in statistical applications, such as correlation algorithms.

3.1.1 Investigation of Diagnostic Methods Used for Health Monitoring

FTT has experience in the health-monitoring sector and holds a U.S. patent for "Method for detecting a defect on an operating turbine rotor blade" (US8413493 B1). This method analyzes real-time IR data to assess an in situ component and makes a determination on whether a defect (such as a plugged cooling hole or coating spallation) is present. See figure 32 for an example of the patented algorithm applied to IR monitoring data of turbine blades. Because of the nature of the transient data that SIR provides, this method was ultimately not considered. There are, however, pattern and geometry identification methods in the algorithm that may prove to be useful in future iterations of the DRA.

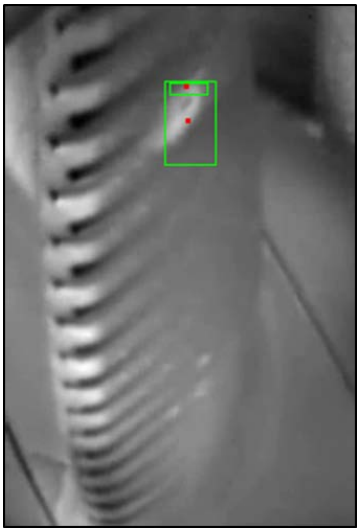

Figure 32. Example of the FTT diagnostic method identifying spallation on a turbine blade

3.1.2 Investigation of Neural Networks and Learning Algorithms

Neural networks and learning algorithms were evaluated because of their success in other industries—in particular, pattern recognition applications. During this part of the survey, neural networks were first evaluated because of FTT's familiarity with them and their ability to program neural networks in code. Neural networks are a black box technique that can learn patterns and identify linear, nonlinear, and discontinuous systems. See figure 33 for a diagram of a neural network. Neural networks also have industry success in health monitoring (e.g., detecting structural damage) and facial recognition.

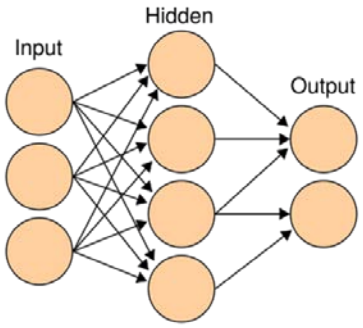

Figure 33. Diagram of a neural network

Next, other learning algorithms were evaluated, specifically fuzzy learning algorithms. These algorithms use rules and empirical knowledge, in conjunction with learning, to model systems. See figure 34 for an example of a fuzzy learning diagram. Fuzzy learning algorithms have industry success in structural health monitoring, such as damage detection in composites, and success in sensor-placement optimization.

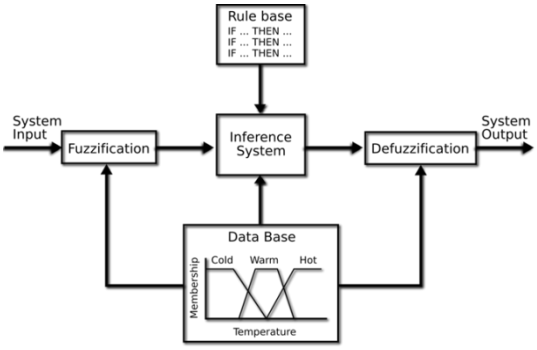

Figure 34. Example diagram of a fuzzy learning algorithm[1]

Both of these health-monitoring methods were evaluated for application to defect recognition. A neural network test code was produced; however, the fuzzy learning algorithm was not coded because the database development and inference system was expected to be very time consuming compared to the other more modest approaches available.

[1] Image acquired from: http://www.cs.bris.ac.uk/~kovacs/publications/gbml-survey/html-version/shadow-fuzzy-inference.png

The neural networks did not perform as well as expected, and getting a neural network to converge on a solution proved to be difficult. Neural networks may still have an application in SIR inspection analysis, but instead of using the entire time-series signal as the input to the neural network, some pre-processing of the input data will be required. This will reduce the number of calculations and weight functions for the neural network, resulting in less time to converge to an answer during the training process.

3.1.3 Investigation of Methods Used in Academia

The academic community has been contributing to the innovation and advancement of SIR from its inception. This survey focused on the research and progress made in the areas of signal processing and modeling advancements at Iowa State University. Two methods in particular were thoroughly investigated: matched filtering [2] and thermographic signal reconstruction [3].

The matched filtering method uses a mathematical convolution process to increase the signal-to-noise ratio of crack indications. This method thereby increases detectability of crack signals, even if the signals are weak or noisy. See figure 35 for a representation of the match filter process method (note that figure 35 was acquired from [2]).

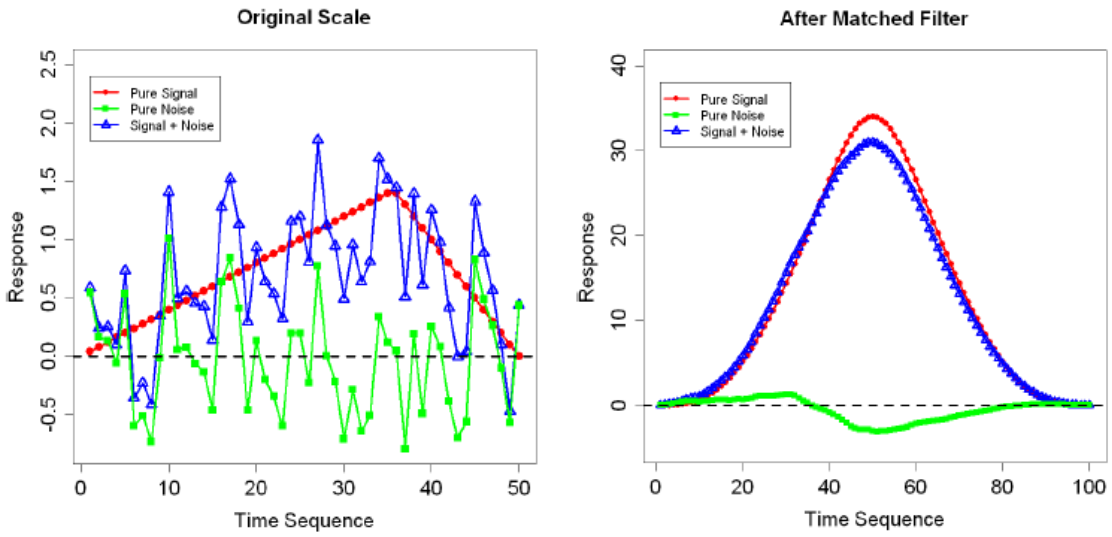

Figure 35. Signal measurements before and after matched filter[2]

The thermographic signal reconstruction method recreates the traditional (theoretical) crack signal that occurs under an SIR inspection. This method uses a physics-based approach to model the heating and cooling signal of a crack. Figure 36 is the final model created from this process (figure 36 was obtained from [3]).

$$
\begin{aligned}
T(t) &= 0 && (t \le t_1)\\
T(t) &= \frac{1}{4\pi\alpha|R|}\left[\operatorname{erfc}\left(\frac{|R|}{\sqrt{4\alpha(t-t_1)}}\right)\right] && (n=3 \text{ and } t_1 < t \le t_2)\\
T(t) &= \frac{1}{4\pi\alpha|R|}\left[\operatorname{erfc}\left(\frac{|R|}{\sqrt{4\alpha(t-t_1)}}\right) - \operatorname{erfc}\left(\frac{|R|}{\sqrt{4\alpha(t-t_2)}}\right)\right] && (n=3 \text{ and } t > t_2)\\
T(t) &= \frac{1}{4\pi\alpha}\left[-\operatorname{Ei}\left(-\frac{|R|^2}{4\alpha(t-t_1)}\right)\right] && (n=2 \text{ and } t_1 < t \le t_2)\\
T(t) &= \frac{1}{4\pi\alpha}\left[-\operatorname{Ei}\left(-\frac{|R|^2}{4\alpha(t-t_1)}\right) + \operatorname{Ei}\left(-\frac{|R|^2}{4\alpha(t-t_2)}\right)\right] && (n=2 \text{ and } t > t_2)\\
T(t) &= \frac{|R|}{4\alpha\sqrt{\pi}}\left[\Gamma\left(-0.5, -\frac{|R|^2}{4\alpha(t-t_1)}\right)\right] && (n=1 \text{ and } t_1 < t \le t_2)\\
T(t) &= \frac{|R|}{4\alpha\sqrt{\pi}}\left[\Gamma\left(-0.5, -\frac{|R|^2}{4\alpha(t-t_1)}\right) - \Gamma\left(-0.5, \frac{|R|^2}{4\alpha(t-t_2)}\right)\right] && (n=1 \text{ and } t > t_2)
\end{aligned}
$$

Figure 36. Thermographic signal reconstruction equations for n = 1, 2, or 3 dimensions[3]

The matched filter process was coded similarly to test how it would fit with the vision of the DRA. Ultimately, matched filtering was not included in the DRA because of its dependence on signal amplitude, but some of the spatial filtering techniques were adopted. The thermographic signal reconstruction method was also coded similarly and proved to be a useful tool in the DRA, especially in conjunction with the correlation methods referenced in the following section. The thermographic signal reconstruction provides the DRA a way to model what crack signals are expected and allows these signals to be compared to the raw SIR inspection data.

3.1.4 Investigation of Correlation Methods

Lastly, the statistical community was surveyed for methods applicable to signal processing of time-series data. Correlation algorithms were a natural choice for focused investigation because they can be used to compare the similarity of signals. With the thermographic signal reconstruction crack model (or an empirical crack signal), raw SIR data can be correlated to the theoretical (or empirical) crack model, and a correlation (similarity) value can be determined. This should mean that signals with cracklike behavior will have high correlation values, and non-cracklike (background, noise, etc.) signals will have low correlation values. A correlation image can be constructed, and crack indications should stand out from the rest.

Two correlation algorithms were useful in the DRA: Pearson's R correlation and Kendall Tau's correlation. The algorithm for Pearson's R correlation can be found in equation 1, and the algorithm for Kendall's tau correlation can be found in equation 2. Note that correlation values typically range from -1 to 1, or 0 to 1:

$$\rho_{X,Y} = \frac{\operatorname{cov}(X,Y)}{\sigma_X \sigma_Y} \tag{1}$$

where cov(X, Y) is the covariance, and σ is the standard deviation:

$$r = \frac{(\text{number of concordant pairs}) - (\text{number of discordant pairs})}{\frac{1}{2}n(n-1)} \tag{2}$$

Other ranked correlation methods were considered (like Spearman's rank correlation), but ultimately not selected, because they were similar variants to the general correlation coefficient. Kendall is a particular case of general correlation (as is Spearman), but its method of concordant pars is an intuitive assessment of the temporal ascent and decay of the cracklike signals.

3.1.5 Conclusions of the Survey

At the conclusion of the survey, a few methods stood out from the rest and became the foundation for the DRA. The foundational methods were: thermographic signal reconstruction, Pearson's R correlation, Kendall tau rank correlation, and spatial filtering techniques from the matched filter method. These were the building blocks for what would become the DRA. See section 3.2 for DRA details.

3.2 DRA

The DRA was developed over the course of approximately 18 months during the contract effort. This section provides details and a full breakdown of the algorithm, both how it works and how it performs. Figure 37 is the flowchart of the algorithm. Each process in the flowchart is detailed in sections 3.2.1–3.2.8.

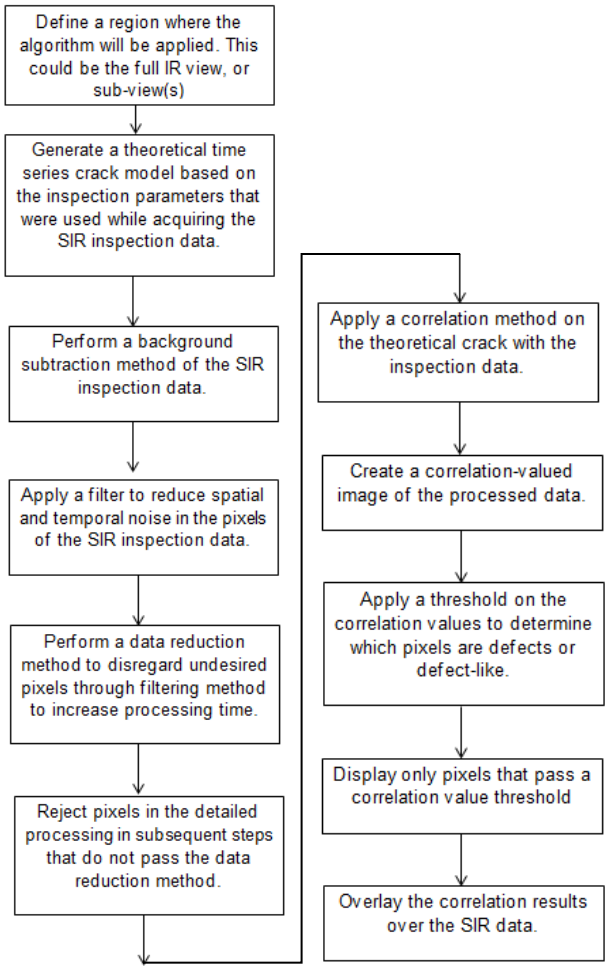

Figure 37. DRA flowchart

3.2.1 Define ROI—Full IR View or Subview(s)

To start the process, the user has the ability to define a region where the DRA will be applied. This could be the entire IR view or subview(s). To create subviews, the users draw a box (or any shape in the code's toolbox) at one or multiple regions. The algorithm will be applied only to those regions. Note that to inspect the entire IR view, the user simply does not draw anything in the IR view. For an example of a user-defined subview, see figure 38.

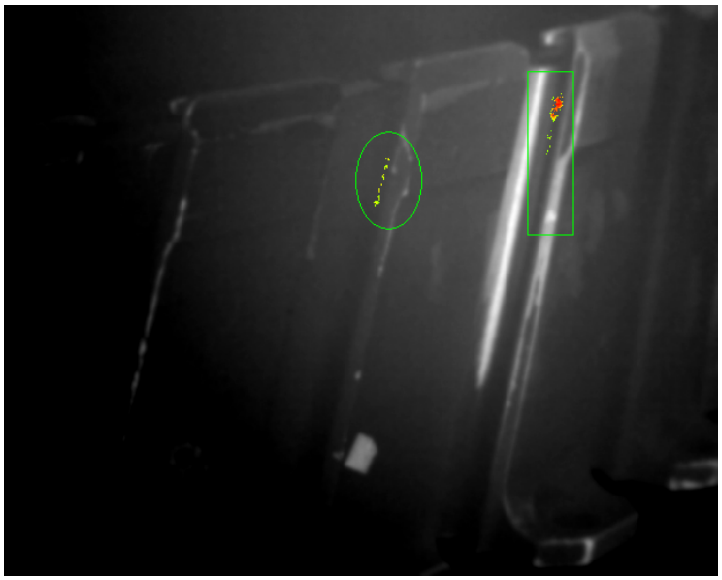

Figure 38. Example of user-defined subviews; DRA results are in color within the subviews

Having the capability to define specific subviews enables the DRA to be flexible for future implementation in SIR software packages. It would not need to be a standalone application. It could be incorporated in the native SIR software package because it has the software hooks necessary for a top-level program to define all of its inputs (such as subviews and thresholds).

3.2.2 Generate Crack Model Based on SIR Parameters

The next step in the algorithm is to define a crack model based on the SIR parameters. The most important SIR parameter is the excitation time—this defines when the crack signal stops heating and starts cooling. The crack modeling method used in this project is the same model developed by ISU[3]. Refer to section 3.1.4 for details about the thermographic signal reconstruction. Figure 39 shows an example of a crack model signal for an excitation time of 0.5 seconds. This crack model will be used in the correlation method later in the algorithm because this model represents how crack signals are expected to behave during the SIR inspection.

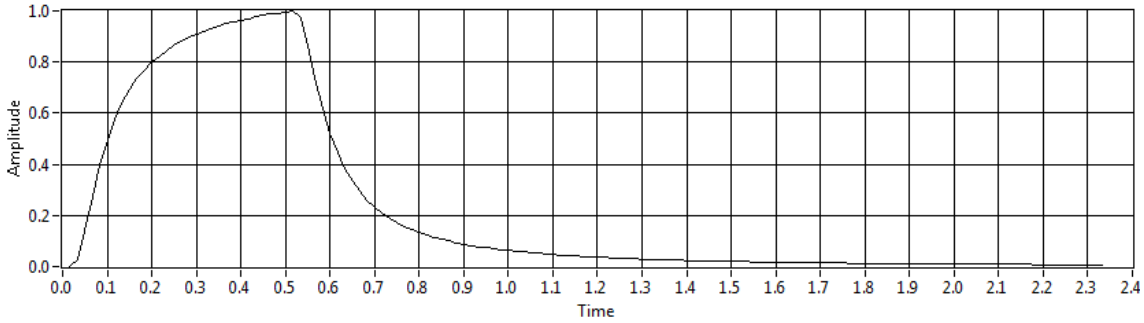

Figure 39. Example of normalized crack model for 0.5 sec excitation time

3.2.3 Background Subtract SIR Inspection Data

When analyzing SIR inspection images, it is more valuable to monitor the change in temperature than just the absolute temperature. For this reason, the next step in the algorithm is to perform a background subtraction, which means subtracting the first frame from all later frames of SIR data. The result reveals the change in the thermal signals over time. Figure 40 shows a snapshot of the benefit in using background subtraction in which only the differential thermal signal is displayed, greatly improving both the visual contrast at the crack location and filtering of the signal for further processing by the DRA.

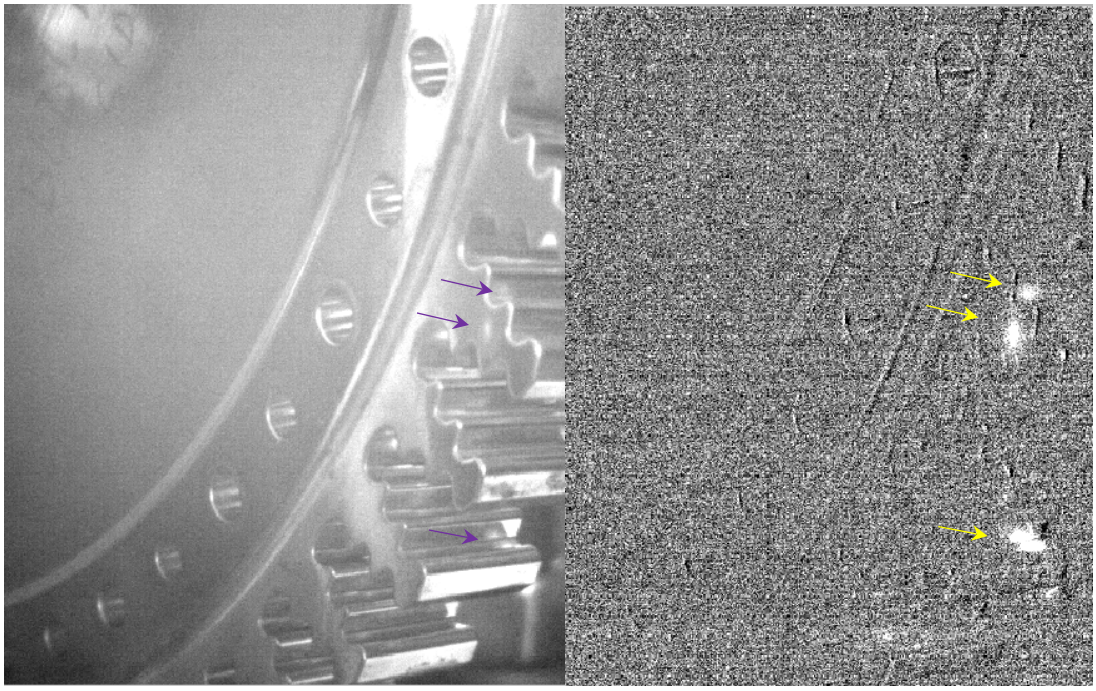

(a) (b)

Figure 40. The raw SIR image of (a) a JT8D disk with cracks in the tangs at the arrows; (b) these cracks appear as white indications using background image subtraction

3.2.4 Apply Filter to Reduce Spatial and Temporal Noise

The data coming from the IR camera is often a little noisy, and when an inspector is trying to find small (faint) cracks, it can be difficult to see clearly. The next step in the algorithm addresses the spatial and temporal noise that occurs with SIR inspection data. Spatial noise can come in the form of hot or dead pixels. Hot pixels usually appear bright, and dead pixels usually appear dark. These troubled pixels output erroneous signals and look like speckles in the SIR viewer. There is also some pixel-to-pixel variation among adjacent pixels. Companies like FLIR, who produce IR cameras, have methods for handling this issue, such as non-uniformity correction (NUC). NUC works well for recalibrating the pixels of the camera, but does not address all of the spatial noise concerns in SIR inspection, such as edge-effects and small reflections. Spatial filtering is an option that can be turned on in the DRA. The spatial filter used is a Gaussian Kernel filter, which helps by smoothing the spatial noise. Figure 41 shows a visual comparison of DRA results with and

without a Gaussian filter. Figure 41(b) appears to be a little blurrier because of the Gaussian Filtering; however, from a signal analysis perspective, this smoothing helps produce less noisy results.

Figure 41. The (a) DRA without Gaussian filter and (b) with Gaussian filter applied

Temporal noise is also a concern because the mid-wave IR cameras are very sensitive, often with sensitivity down to 20 mK. Because a typical crack heats up only a degree or two, the noise from the sensitivity of the camera can generate non-smooth heating/cooling profiles. To help mitigate the issue of temporal noise, a time-series moving average filter is applied. The moving average filter was selected over such alternatives as a low pass filter because it does not add time-lag to the processed signal. For SIR inspection data, it is important to maintain the phase of the signal, especially for the data-reduction methods described in section 3.5. Figure 42 shows the signals of pixels that encompass a crack, without any temporal filtering. Figure 43 shows the signals when a moving average filter is applied to this same data.

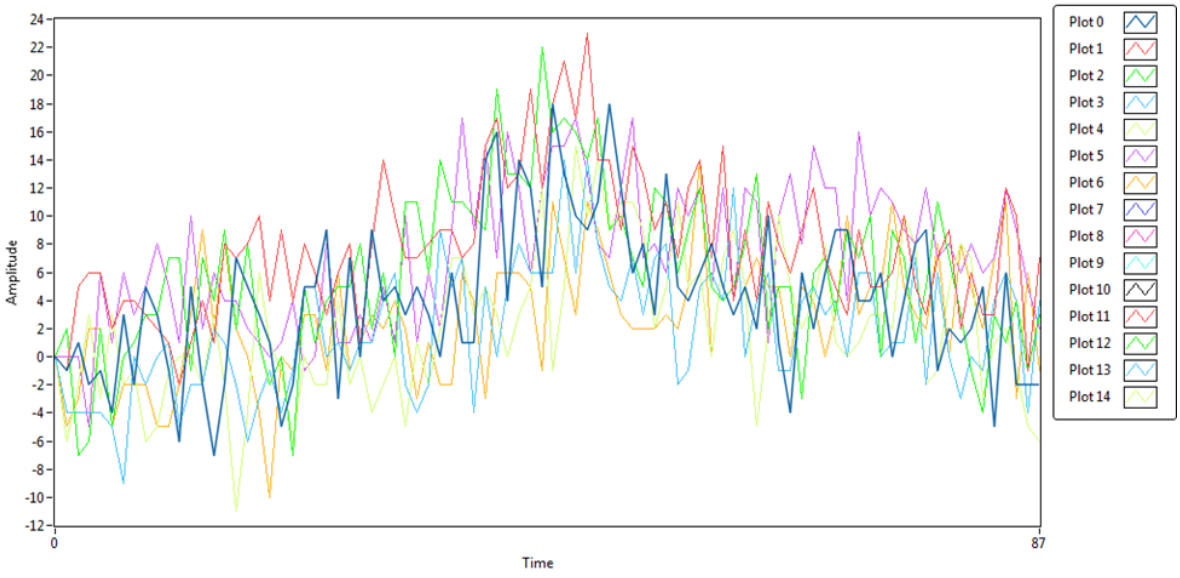

Figure 42. SIR data signals of a crack (individual pixels plotted)

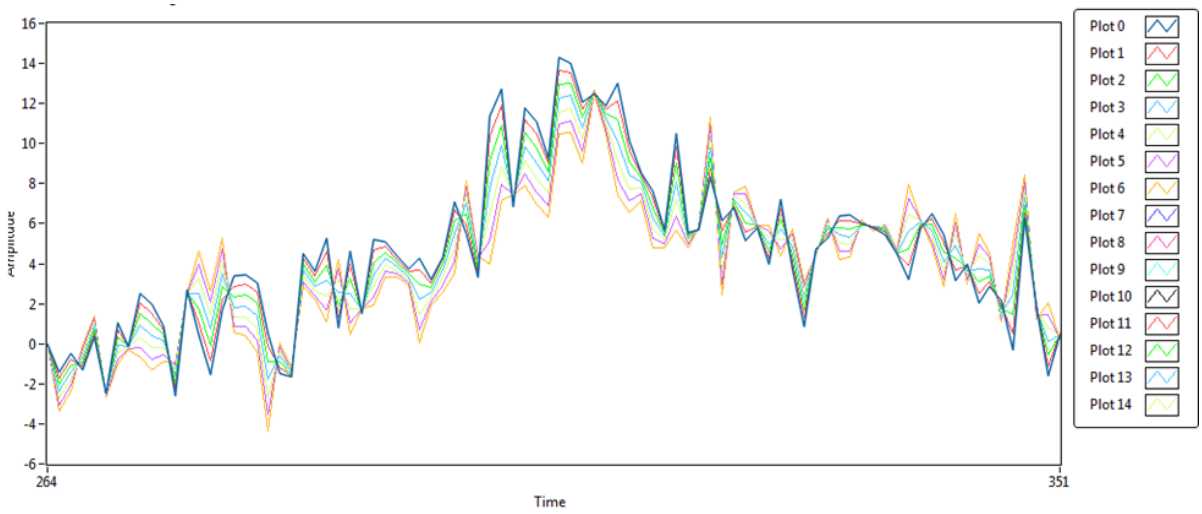

Figure 43. SIR data signals of a crack with time-series moving average filter applied (individual pixels plotted)

3.2.5 Data Reduction

In an effort to decrease the processing time of the DRA, data-reduction methods are applied. These data-reduction methods determine which individual pixels from the SIR inspection data are relevant for the intensive processing that will occur downstream in the DRA algorithm. The data-reduction methods are simple, smart, and help reduce the data to only those pixels that have the general features of a relevant indication.

The first data-reduction method is actually the process described in section 3.1 in which user-defined regions reduce the amount of data the algorithm must process. The next data-reduction method used is peak signal amplitude windowing, which simply means that, based on the SIR excitation time-parameter, there is an expected window in time when the peak signal of a crack indication is expected. For example, if the excitation time parameter is set to 0.5 seconds, a window could be applied that only allows data that falls within +/- 0.1 seconds of the peak time of 0.5 seconds to be included. Figure 44 shows an example of how peak signal amplitude windowing is used: if a pixel's maximum signal occurs within the window, it will continue to the downstream DRA process; however, if the max signal occurs outside the window, it will be reassigned a value of zero and will not continue through the algorithm.

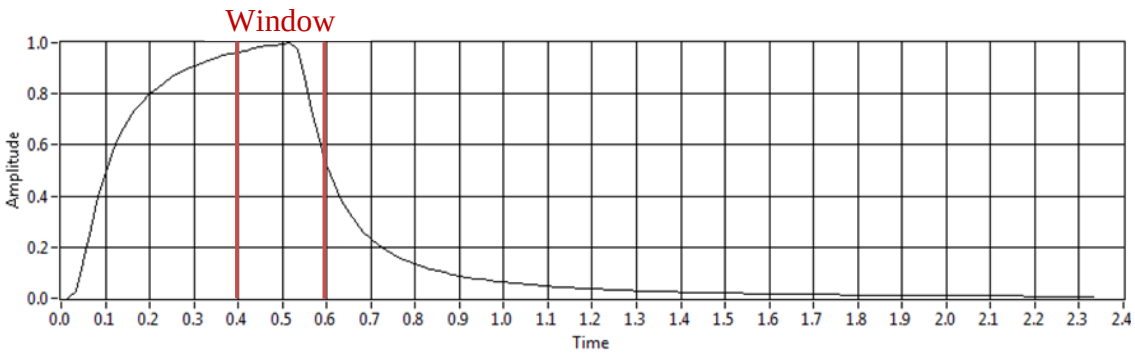

Figure 44. Example of peak signal amplitude window

3.2.6 Apply Correlation Methods

At this point in the algorithm, the SIR pixel data have been filtered and reduced to only the most likely relevant indications. To determine if any of these remaining pixels are relevant indications, the data are applied to a two-step correlation process. The first step is to apply the Pearson's R correlation method by comparing each pixel's data to the crack model previously defined in section 3.2. Pearson's method is computationally fast but less accurate than Kendall's ranked correlation process. For this reason, Pearson's R correlation is used as a pre-filter to Kendall, such that if data from a pixel pass the threshold set for Pearson, then they will proceed to Kendall.

Kendall's rank correlation is computationally intensive and has the ability to correlate linear and nonlinear relationships between two signals. Because the Kendall method is applied only to the pixels that pass the Pearson method, the computational time is reduced. Reducing computational time is important when speed or throughput is important, as in a production inspection process.

For more information about Pearson and Kendall correlation methods, refer to section 3.1.4.

3.2.7 Create Correlation-Valued Image

After all the data have been processed through the appropriate filtering, data-reduction, and correlation calculations, a correlation-value image can be created. The correlation image created by the DRA will contain values that range from 0 to 1. Pixels that did not pass the data reduction or Pearson pre-filter are given a correlation value of zero. Each of the remaining pixels that went through the entire DRA will have some value between 0 and 1. This correlation image does not necessarily need to be exposed to the user; section 3.2.8 will describe a better method for presenting the data. However, for a better understanding of the DRA, figure 45 shows what a correlation image can look like for an SIR inspection of a disk with a defect. Note that in figure 45, blue means low correlation and red means high correlation.

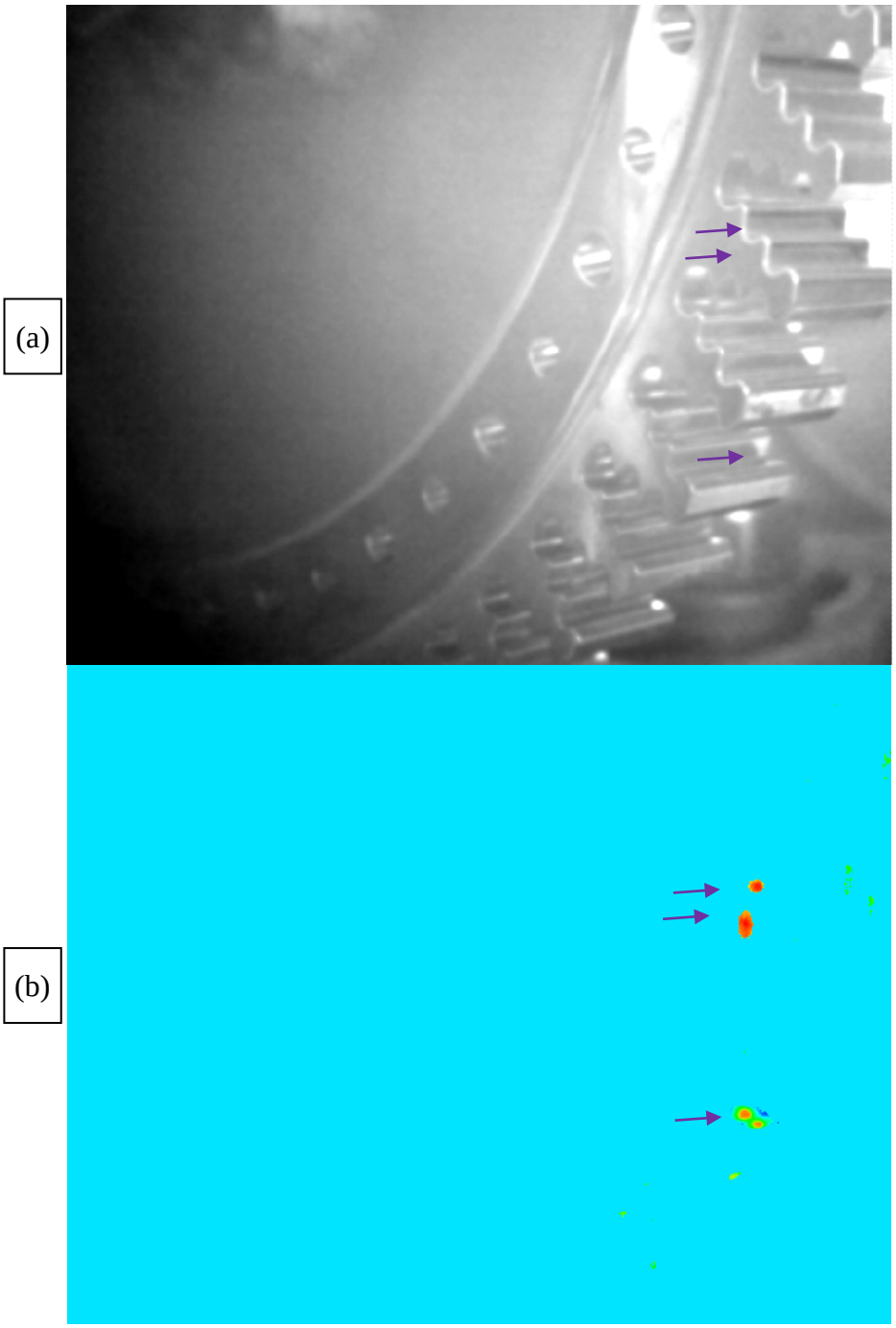

Figure 45. Correlation-value image of a JT8D disk with crack indications: (a) SIR view of JT8D and (b) corresponding correlation-value image

3.2.8 Process and Display Results to the User

In an effort to make the correlation data easier to visually interpret, a threshold can be applied on the correlation-value image. Only the pixels that pass the threshold (e.g., only pixels greater than 0.50) will get color overlaid onto the first frame of the SIR inspection. This provides good contrast

because the SIR data are represented in black and white and the correlation-value data are represented with a rainbow-color map (blue, green, yellow, orange, red). Figure 46 shows what the processed overlay image looks like to the user. Note that figure 46 is the same data presented in figure 45.

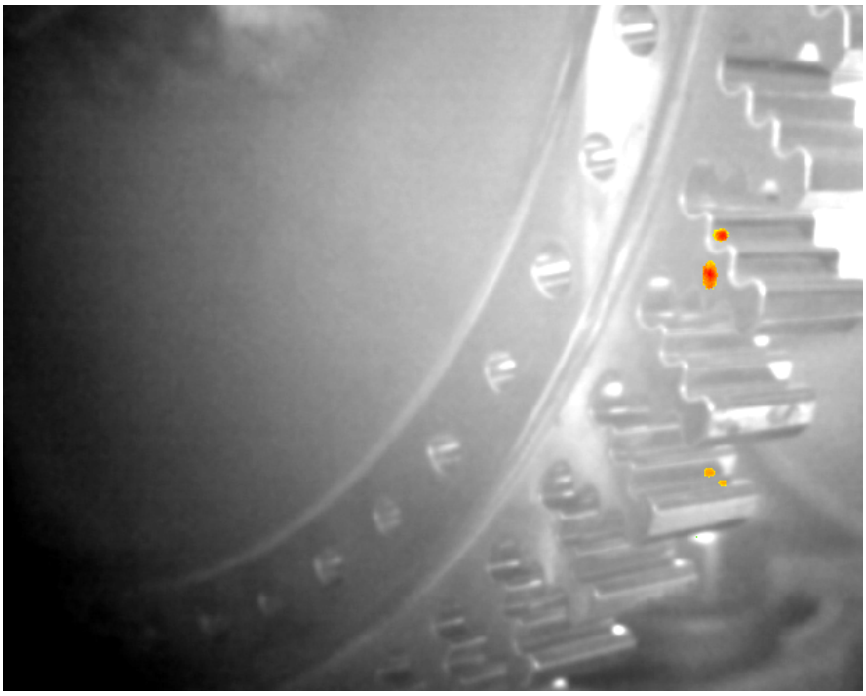

Figure 46. DRA image result of JT8D disk with crack indications

This concludes the description of how the algorithm functions. Anecdotally, the algorithm appears to pick up almost every crack indication within view. There are scenarios in which cracks are too faint and the algorithm may not pick up the defect. In such cases, it should be possible to further optimize the DRA parameters accordingly. Test trials indicate this DRA meets the goal of the current effort—advance the SIR technology platform through algorithm-assisted determination of indications to help improve inspection reliability. The DRA's computational time is dependent on the number of defects it needs to process and the length of the excitation time. Typical inspections, with 0.5–1.0 second of excitation time and with a handful of defects, can take 3–10 seconds to process on a standard laptop. This processing time is reasonable for a production environment.

Implementation of the DRA will result in several inspection advantages by minimizing subjective inspector interpretation of nondestructive testing (NDT) information. This issue was noticed and addressed for eddy current inspection years ago when the USAF made a commitment to fully automate eddy current inspection for engine parts at its overhaul depot. It is clear that skilled automation of data analysis and presentation enhances NDT reliability by eliminating, or at least minimizing, inspector bias and fatigue. A lower false call rate is also achieved when the inspection threshold is properly applied in conjunction with automation of data analysis and presentation. Naturally, if system calibration is done consistently, then system-to-system variability is negligible. This is reflected in consistent NDT reliability demonstration results for the eddy current systems. The same result is anticipated for multiple copies of an SIR testing system.

To summarize, some of the obvious benefits of the DRA with its improved image analysis accuracy are to:

- Minimize missed indications.
- Add uniformity to the identification of “real defects.”
- Minimize false calls.
- Improve system-to-system reproducibility in defect detection.

Less obvious benefits of the DRA are to reduce the influence of operator discretion or bias from operator guided image analysis. The DRA will put fewer demands on the operator for a good image analysis and will therefore reduce operator fatigue and resulting errors.

Appendix B contains additional DRA results for different disk types that were inspected.

3.3 SUMMARY OF DRA

The DRA development effort produced a useable and well-performing tool for assisting inspectors in analyzing SIR inspection data. The evolution of the algorithm began with a survey of industry and academia for existing signal-processing and analysis methods. From the survey results, selected methods were used as the foundation for the algorithm. The algorithm then matured to incorporate filtering and data reduction to increase performance by both decreasing processing time and by handling the inherent noise (spatial and temporal). In the end, the full algorithm can produce color-mapped overlay images that clearly depict where the algorithm determines relevant indications are located. This visualization makes it easy for an inspector to understand where the indications are located and a relative confidence level on whether the indication is relevant (blue is low confidence, and red is high confidence). Overall, the DRA is at a point at which it can be used to reduce the human variability of making a decision while inspecting engine components for surface cracks.

Reference appendix B for additional DRA results of different disk types, which include APU Disks, F110 Fan Disk, and JT8D Turbine Disk.

4. SIR IMPLEMENTATION TOOL

4.1 BACKGROUND

Based on experience with numerous applications, a flow chart and software tool were developed for the implementation of SIR for different components. Specifically, the SIR implementation tool addresses three styles of components: disks, blades, and generic components. The goal of the flowchart and software tool (which are identical in function) was to provide operators a set of initial SIR parameters that would be suitable as a starting point for optimizing an inspection for that particular component. Each different component could require different parameters under SIR. Examples of typical parameters that need to be tuned for a component are excitation time and excitation amplitude.

4.2 GENERATION OF QUESTION/ANSWER RULES

At the heart of the SIR implementation tool is a flowchart process by which inputs (or combinations thereof) determine unique outputs for the users. These outputs are parameters, settings, or suggestions for optimizing an SIR inspection for a particular component. A question/answer (Q/A) list is an abstraction of the flowchart and an easier starting point for laying down the foundation of the SIR implementation tool. Because three component styles were selected for this program (disks, blades, and generic), three Q/A lists were generated. This Q/A list makes the generation of a flowchart and software tool easier to implement because it serves as the blueprint for the tool. Sections 4.2.1–4.2.3 detail the Q/A lists for disks, blades, and generic components.

This is the first, preliminary construction of a SIR implementation tool, which is a "living document." As experience is gained by this team, refinements will be made. In addition, it will be provided to aircraft NDT experts for comments and questions. These will be people with only cursory knowledge of SIR testing. That feedback will be valuable in refining the tool so that the new practitioner can get much farther and make rational decisions without being tied to a small group of SIR engineers at the early stages of implementation. In fact, there will be some cases in which use of the tool will allow the new practitioner to eliminate SIR testing as the most applicable NDT method without spending an extraordinary amount of time in the initial stage.

4.2.1 Q/A List for Disks

The following Q/A list is for disks:

1. Are the users inspecting for surface cracks, delamination, voids, porosity, etc.?

    a. Only proceed if the answer is cracks.

2. Inspecting the entire part or a known area?

    a. Entire part: may require multiple camera views, likely multiple fixtures.
    b. Known area: may require a few views, likely a single fixture.

3. What size crack is the user looking for?

    a. Determines distance of camera for proper field of view (FOV) and time of excitation.

4. How big is the disk or local area being inspected?

    a. Determines number of inspection views given the FOV and area.

5. What material is the disk?

a. Helps determine the amplitude of the exciter.

6. Are there existing attachment features on the disk, such as flanges, integral arms, or bolt holes in the bore, web, or rim of the disk?

   a. Determines the component's fixture location and design.
   b. If the answer is YES:

      i. Bore Flange >> Design a support to attach here, which is also fixed to ground.
      ii. Web Flange >> Design a support to attach here, which is also fixed to ground.
      iii. Rim attachment >> Design a support to attach here, which is also fixed to ground.
      iv. Bolt holes >> Design a fixture to mate/align with bolt pattern, which is also fixed to ground.

   c. If the answer is NO:

      i. Design a compression fixture that does not damage the component (e.g., clamping the bore).

7. Are there flat locations on the disk that are located in lower stress regions?

   a. If the answer is YES:

      i. Suggest to impact there, the horn should be perpendicular, include an interface layer, and suggest impacting away from the fixture points.

   b. If the answer is NO:

      i. Impact interface component needs to be created to provide a flat contact with the horn.

   c. If the answer is YES or NO:

      i. Provide suggestions for interface materials (e.g., cardstock).

   d. Caution: Do not impact seals.

4.2.2 Q/A List for Blades

The following list is for blades:

1. Are the users inspecting for surface cracks, delamination, voids, porosity, etc.?
    a. Only proceed if the answer is cracks.
2. Inspecting the entire part or a known area?
    a. Entire part >> multiple camera views, likely multiple fixtures.
    b. Known area >> a few views, likely a single fixture.
3. What size crack is the user looking for?
    a. Determines distance of camera for proper FOV and time of excitation.
4. How big is the blade or local area being inspected?
    a. Determines number of inspection views given the FOV and area.
5. What material is the blade?
    a. Helps determine the amplitude of the exciter.
6. Turbine or Compressor Blades?
    a. Determines the component's fixture location and design. Typical design for blade fixture is a hardened pinch block.
    b. If the answer is Turbine:
        i. Above Platform Fixture >> Grip the fir tree.
        ii. Below Platform Fixture >> Grip platform and dampen the motion of the airfoil.
    c. If the answer is Compressor:
        i. Above Platform Fixture >> Grip the dove tail.
        ii. Below Platform Fixture >> Grip platform and dampen the motion of the airfoil.

4.2.3 Q/A List for Generic Components

The following Q/A list is for generic components:

1. Are the users inspecting for surface cracks, delamination, voids, porosity, etc.?

    a. Only proceed if the answer is cracks.

2. Inspecting the entire part or a known area?

    a. Entire part >> multiple camera views, likely multiple fixtures.
    b. Known area >> a few views, likely a single fixture.

3. What size crack is the user looking for?

    a. Determines distance of camera for proper FOV and time of excitation.

4. How big is the component or local area being inspected?

    a. Determines number of inspection views given the FOV and area.

5. What material is the component?

    a. Helps determine the amplitude of the exciter.

6. Are there existing attachment features on the component like flanges, integral arms, or bolt holes?

    a. Determines the component's fixture location and design.
    b. If the answer is YES:

        i. Flange >> Design a support to attach here, which is also fixed to ground.
        ii. Rim attachment >> Design a support to attach here, which is also fixed to ground.
        iii. Bolt holes >> Design a fixture to mate/align with bolt pattern, which is also fixed to ground.

    c. If the answer is NO:

        i. Design a compression fixture that does not damage the component (e.g., clamping the component.)

7. Are there flat locations on the component that are located in lower stress regions?

    a. If the answer is YES:

i. Suggest to impact there, the horn should be perpendicular, include an interface layer, and suggest impacting away from the fixture points.

b. If the answer is NO:

i. Impact interface component needs to be created to provide a flat contact with the horn.

c. If the answer is YES or NO:

i. Provide suggestions for interface materials (e.g., cardstock).

d. Caution: Do not impact seals.

4.3 SIR IMPLEMENTATION FLOWCHART

As a result of defining the Q/A rules, flowcharts can be created that guide users of the SIR implementation to a set of recommended parameters. Ultimately, two flowcharts were defined: one for blades and one for both disks and generic components.

4.3.1 SIR Implementation Flowchart—Disks and Generic Components

Figure 47 is the SIR Implementation flowchart for disks and generic components.

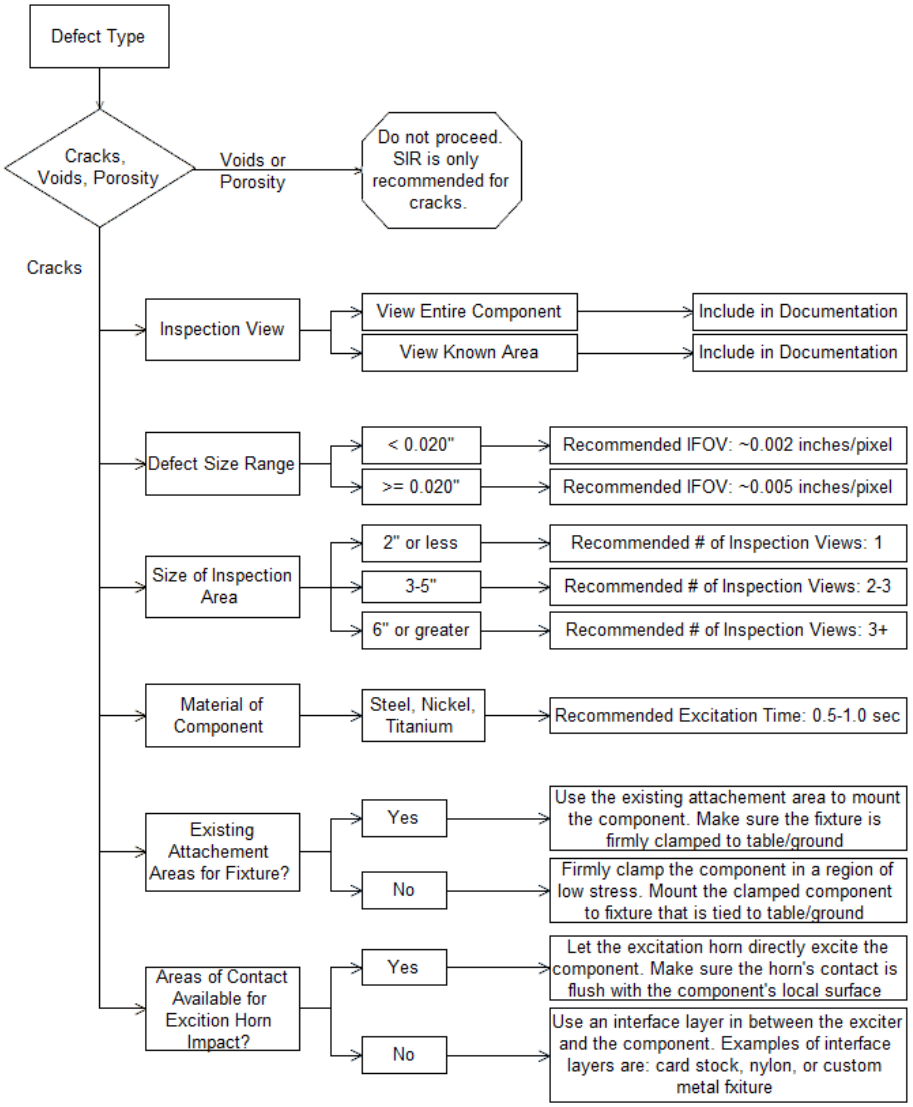

Figure 47. SIR Implementation flowchart—disks and generic components

4.3.2 SIR Implementation Flowchart—Blades

Figure 48 is the SIR implementation flowchart for blades.

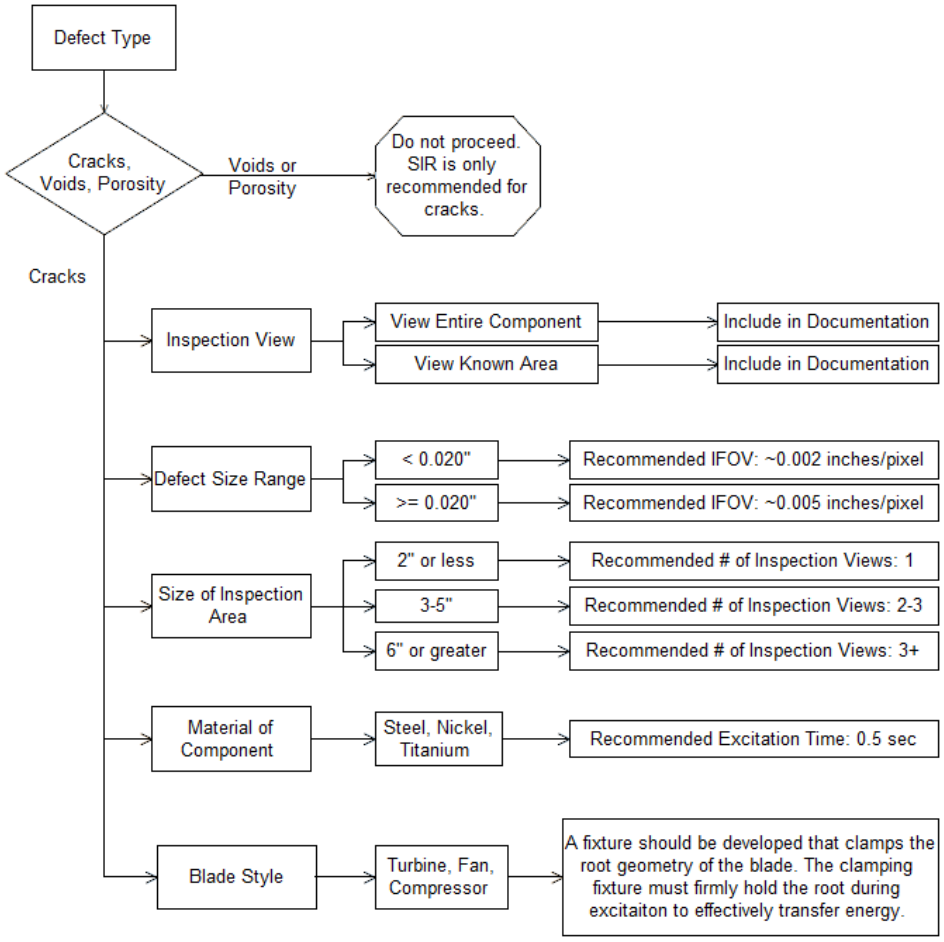

Figure 48. SIR implementation flowchart—blades

4.4 SIR IMPLEMENTATION SOFTWARE TOOL

Using the flowcharts as a blueprint, software was developed to create an SIR implementation software tool. This software tool is an interactive version of the flowcharts, but it also generates a report for the users. This report provides a summary of their selections, provides recommendations for parameters, and also provides an example picture of a similar SIR setup. An example of a SIR Implementation Software Tool Report is found in appendix C.

Figures 49–52 detail the software's simple user interface.

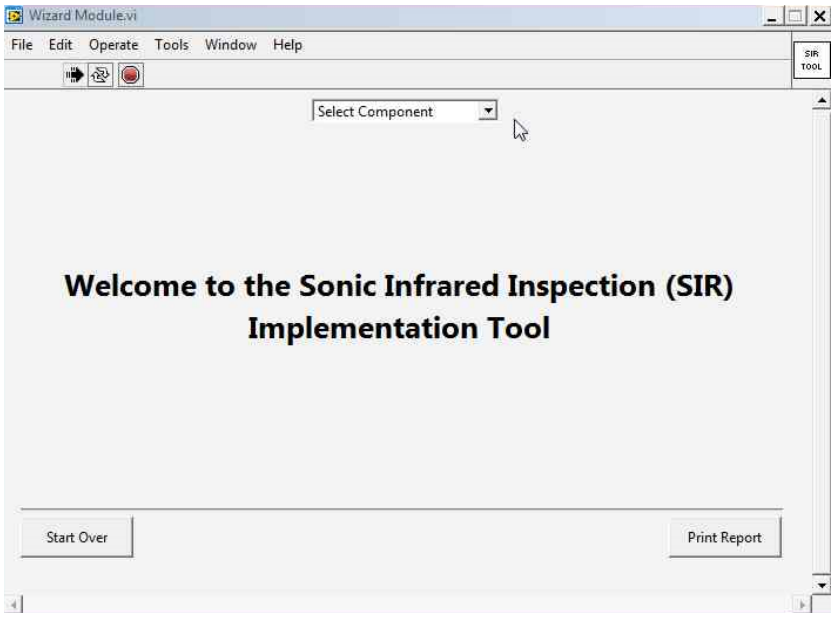

Figure 49. SIR Implementation Software Tool Welcome Page

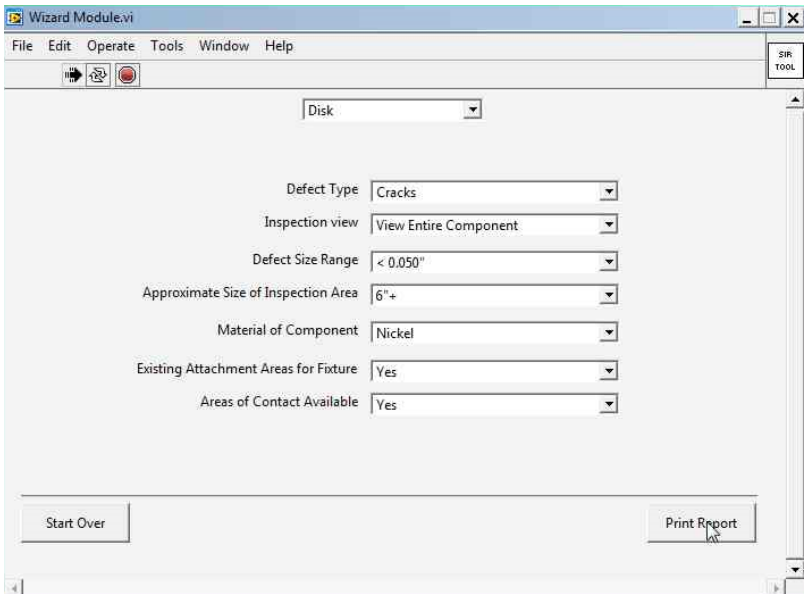

Figure 50. Example of selections for disk

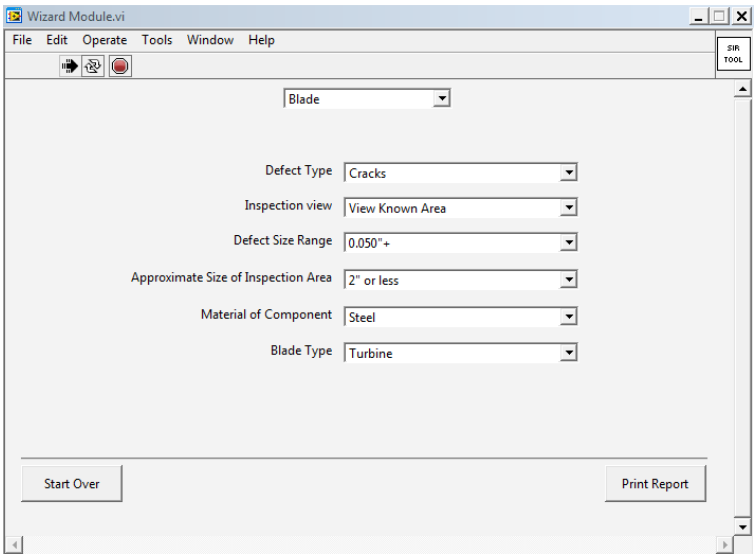

Figure 51. Example of selection for blades

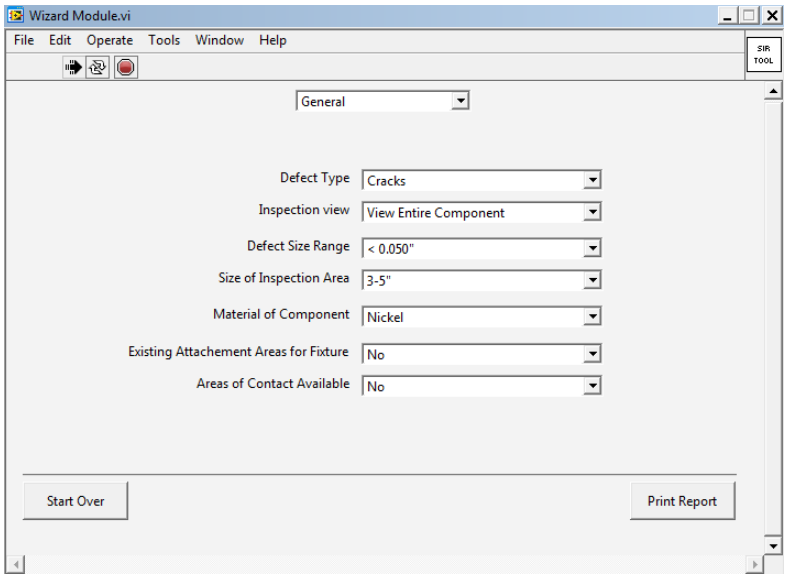

Figure 52. Example of selection for generic component

4.5 SUMMARY OF SIR IMPLEMENTATION TOOL AND FLOWCHART

The creation of these two tools (flow chart and software tool) will help users of the SIR inspection technique better determine a starting point for new components or new applications of the system. This will encourage the development and use of SIR and will hopefully have an impact on improving the consistent application of the inspection process.

5. HYBRID CAMERA DESIGN–VISIBLE AND INFRARED

5.1 BACKGROUND

In an effort to improve the presentation and documentation of SIR image data, a hybrid camera concept was explored. This hybrid camera will acquire IR and visual data from the same perspective to form a single hybrid image. Therefore, this image will then contain information from both wavelength ranges (visible and infrared). The data in this one image are represented as the following: the DRA results overlay the visible image. This provides improved contrast and color over the previous documentation that only included DRA results overlaid on IR data. Because IR is only sensitive to temperature, components that are close to isothermal with high emissivity can appear blurry or lack contrast. The hybrid camera's visible image replaces the underlying image in full color and focus. This makes it easier for the users to locate and evaluate potential defects.

5.2 IR CAMERA

The IR camera that was procured for this program was the FLIR A6700sc. It is a MWIR camera (standard for the SIR application) with a resolution of 640 x 512 at 60 frames per second (FPS). At the date of purchase, the A6700sc was the latest generation of MWIR camera in the FLIR suite. Table 1 details the specs of the A6700sc. Figure 53 is a photograph of the camera.

Table 1. FLIR A6700sc specifications

Feature	Specification
Detector Type	Indium Antimonide (InSb)
Spectral Range	3.0–5.0 µm
NETD	<20 mK
Frame Rate	60 Hz
Camera f/#	4.0
Output Format	GigE Vision
Weight	5 lb

Figure 53. FLIR A6700sc camera

5.3 VISIBLE CAMERA

The visible camera that was procured for the program was a Genie TC-C2500. This camera was selected because of the following traits: resolution and output format. The resolution of the camera is exactly double (in both the rows and the columns of pixels), thereby making any image overlay a simple double (or halving) pixel transformation. The output format for the visible camera is GigE Vision. Therefore, integrating the visible camera and the IR camera is as simple as porting the units through an Ethernet router. Table 2 details the specification of the visible camera. Figure 54 shows the Genie TS-C2500 unit.

Table 2. Genie TS-C2500 specifications

Feature	Specification
Resolution	2560 x 2048
Total Data Rate	320 MB/s
Max. Frame Rate	29 fps
Pixel Size	6 µm
Output Format	GigE Vision
Size	49 x 49 x 56 mm
Mass	200 g

Figure 54. Genie TS-C2500 camera

5.4 HYBRID CAMERA DESIGNS AND DOWN-SELECTION

Originally, three conceptual designs for integrating the visible camera and creating a hybrid camera system were developed. Later in the program, a fourth concept was considered. The details of all four concepts are shown below. Concepts #1, #3, and #4 were studied and their results are described in section 5.5. Concept #2 did not pass the down selection because of the anticipated complexity of the required mounting hardware and the potential challenge of repeatability.

- Concept #1 (see figure 55)
  - Side-by-side arrangement
  - Lateral linear rails to move cameras into position

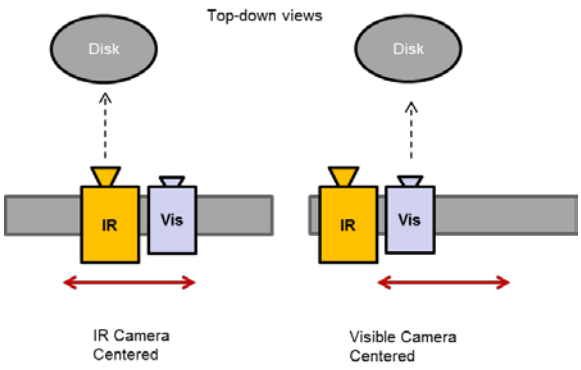

Figure 55. Hybrid camera concept #1

- Concept #2 (see figure 56)
  - Stacked arrangement
  - Tripod z-axis rail to move cameras into position

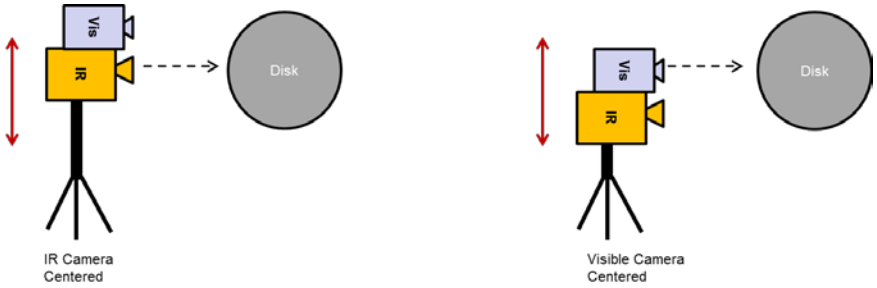

Figure 56. Hybrid camera concept #2

- Concept #3 (see figure 57)
  - Fixed-camera arrangement with pivoting mirror

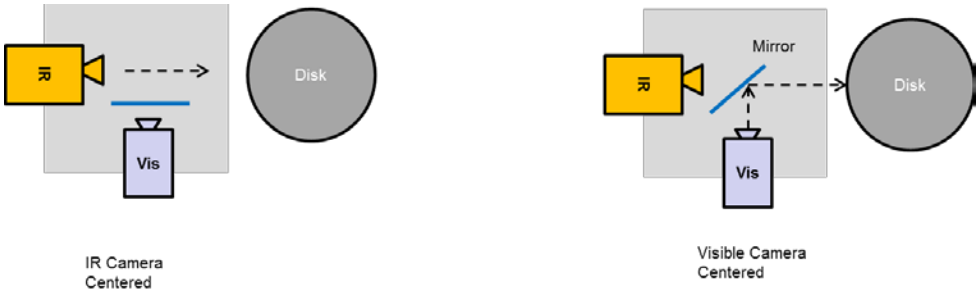

Figure 57. Hybrid camera concept #3

- Concept #4 (see figure 58)
  - Pivoting camera arrangement

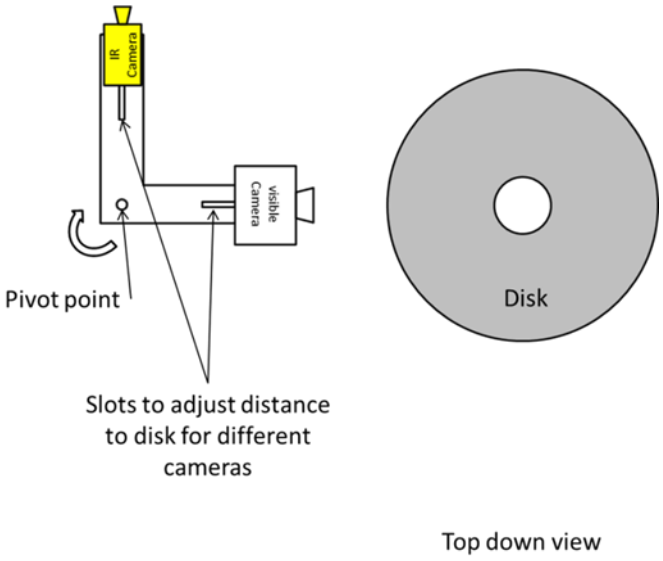

Figure 58. Hybrid camera concept #4

5.5 HYBRID CAMERA RESULTS

5.5.1 Concept #1 Implementation and Results

The design concept for the hybrid camera used a mirror angled at 45º relative to the two cameras (which themselves face 90º apart).

The design includes a custom mirror frame, metal post, and nylon swivel bearing. The mounting bracket is a simple plate with mounting-hole patterns to accommodate the attachment points of the IR camera and the visible camera's rack-and-pinion movement. See figure 59 for a view of this hybrid design.

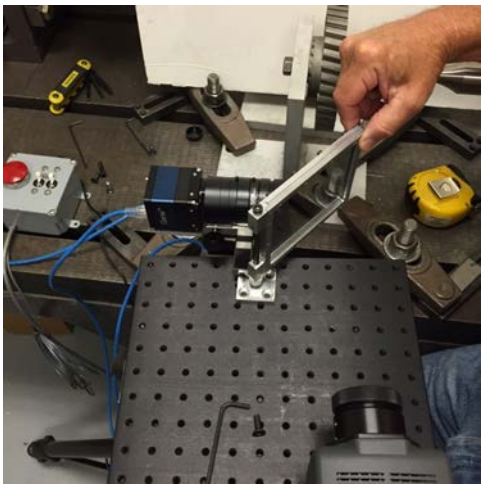

Figure 59. Hybrid camera concept with mirror implemented

This configuration's image overlay appears skewed and is not aligned perfectly. See figure 60 for the overlay results. This is likely due to the numerous mismatches within the lens, detectors, and focal distances. Including the additional complexity of the mirror made for a more difficult alignment of the overlay.

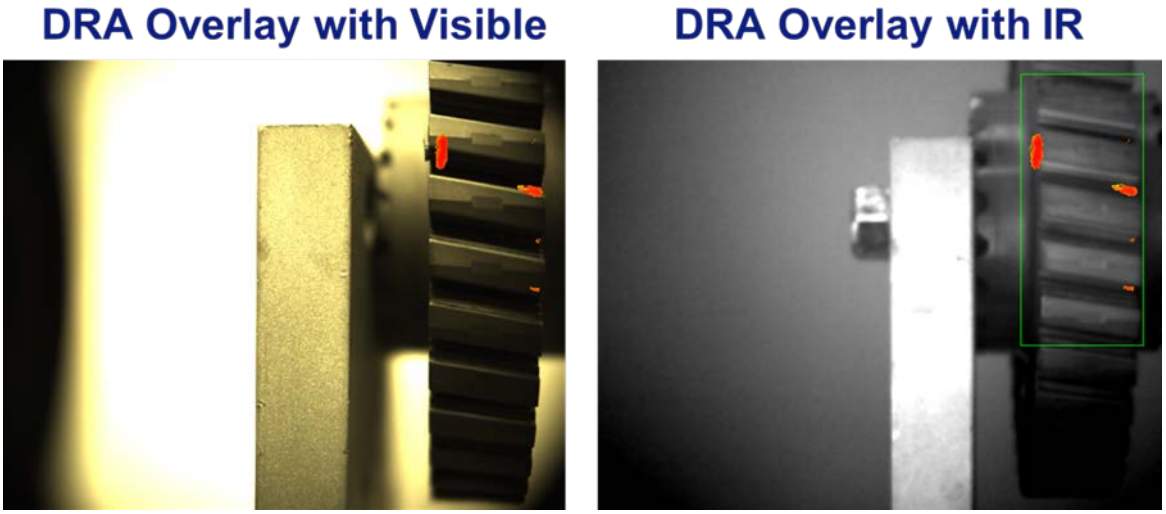

Figure 60. Hybrid camera results for concept #1

5.5.2 Concept #3 Implementation and Results

The design concept for the hybrid camera uses a side-by-side configuration. This means that the whole unit must slide laterally to center each camera. See figure 61 for a view of the new hybrid design.

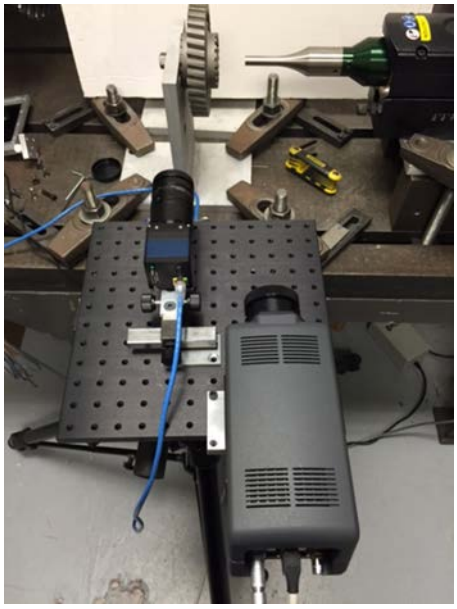

Figure 61. Hybrid camera concept side-by-side implemented

This configuration relatively improved image overlay capability compared to the previous mirror design. See figure 62 for the overlay results. Note that the overlay is still offset, which is likely because of the physical differences in detector size and lens mismatch. The repeatability is also hindered by the inaccuracies of sliding the whole unit side-to-side. An improvement of this design would be to mount the system on a graduate slide rail system such that lateral position could be more repeatable.

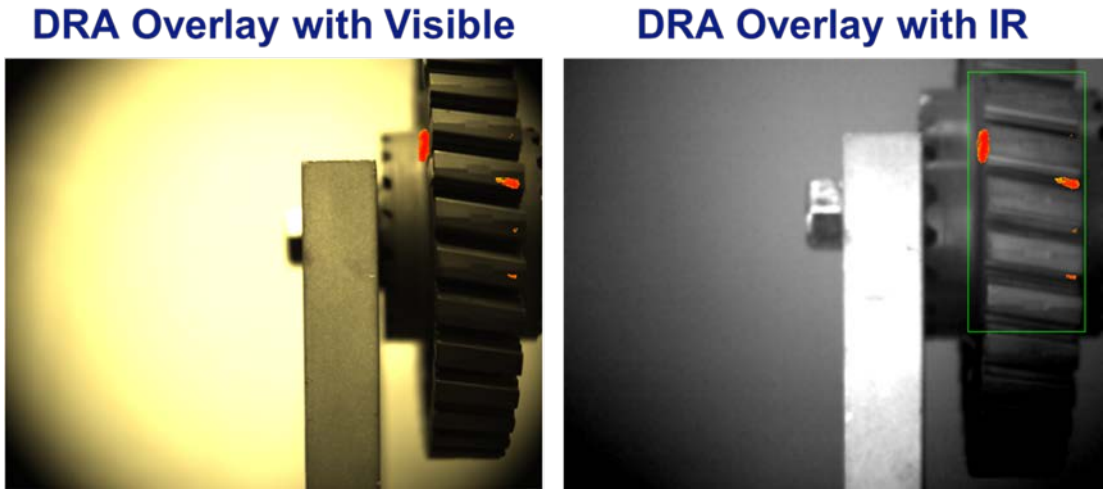

Figure 62. Hybrid camera results for concept #3

5.5.3 Concept #4 Implementation and Results

The design concept for the hybrid camera used a rotational alignment concept with the two cameras facing 90º apart.

The design includes mounting brackets, cam stops, and nylon. The mounting bracket is a simple plate with mounting-hole patterns to accommodate the attachment points of the IR camera and the visible camera's rack-and-pinion movement. See figure 63 for a view of the new hybrid design.

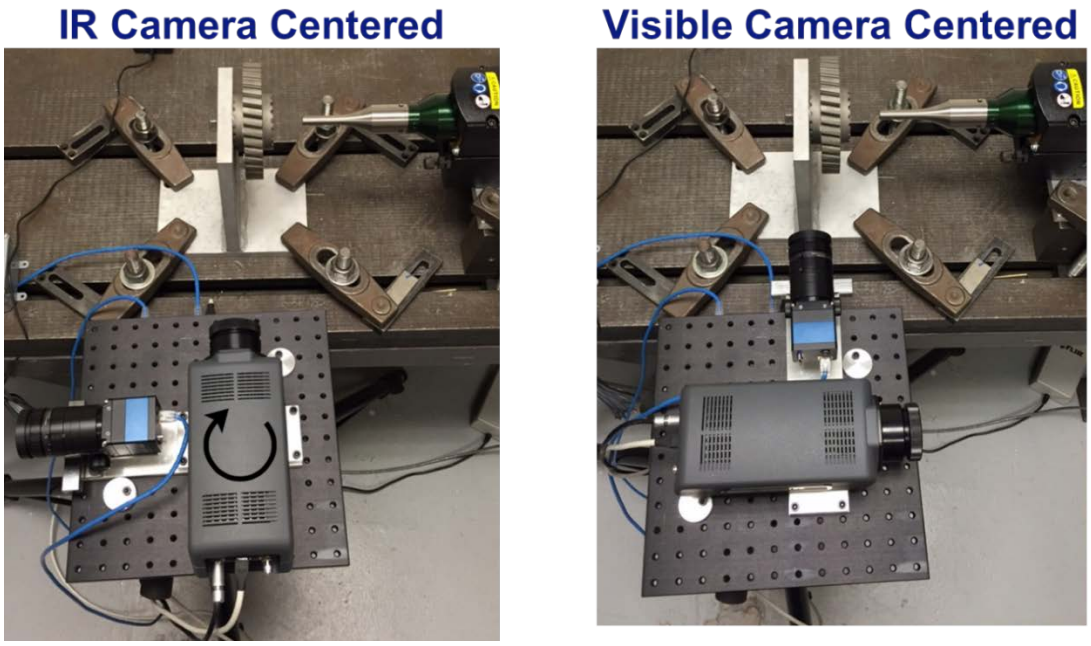

Figure 63. Rotational hybrid camera implemented

This configuration relatively improved image overlay capability compared to the previous designs. See figure 64 for the overlay results. Note that whereas the overlay is still not perfect, it will not ever be due to the physical differences in detector size and lens mismatch. This design also proved to be more repeatable than previous designs. The cam stop was tuned and locked for near perfect 90º rotational repeatability.

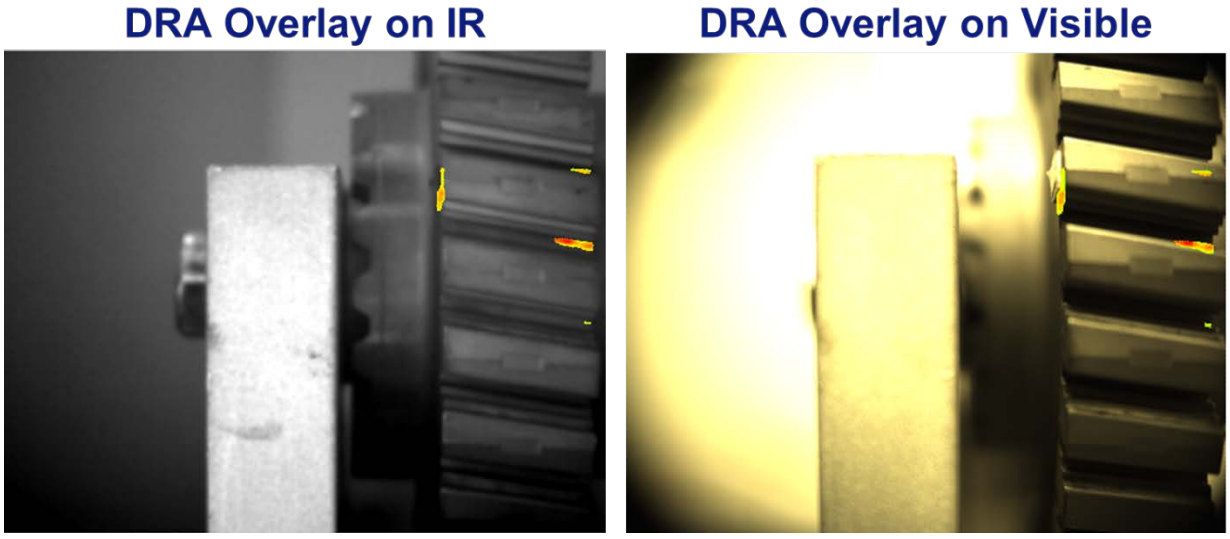

Figure 64. Hybrid camera results for concept #4

5.5.4 Hybrid Camera Conclusions

In the end, the hybrid camera design that proved to be the most repeatable, with regard to camera positioning and consistent overlay, was Concept #4. The pivoting camera arrangement with cam stoppers offered a more intuitive and repeatable process for acquiring both the visible and IR camera data than the other options that were tested. This conclusion was drawn by comparing the aligned images from all four candidates. The difference was so great that detailed measurement of image misalignment was not necessary. Optical comparison of misalignment was obviously the least with Concept #4. Repeatability testing also showed the least misalignment when images from Concept #4 were compared to repeatability testing of images from all the other approaches. True positioning of the hybrid system images will be particularly important when physical examination of specific locations of engine components is necessary to make a final accept/reject call. The other hybrid camera concepts were less reliable because of either human inconsistency in positioning (like the side-to-side concept) or too many degrees of freedom (like the mirror concept).

6. CONCLUSIONS

The following are the conclusions drawn from this study:

- Set screws are a viable option for sonic infrared (SIR) artificial defects (ADs), especially for thick components for which drilling and tapping is possible. This conclusion was drawn based on simple optical comparison of signal amplitude versus time data.
  - The IR responses from the set screws are within range of the cracks' signals
  - The heating and cooling profiles are well behaved and trend like the cracks
  - Press-fit pins are also a viable options and were verified in a different contract (FA8650-10-D-5210) but for the application of ADs for blades
- The testing and results of the AD study showed that most locations on a typical simple engine disk can be excited by SIR. This conclusion was drawn based on the fact that the ADs produced clearly visible signals regardless of disk location.
  - Fixture, excitation time, and excitation amplitude must be set properly, because these parameters tend to vary from disk to disk.
- The defect recognition algorithm (DRA) developed under this program improves the capability of SIR inspections by providing users with areas of interest that statistically represent relevant indications. This conclusion was drawn based on numerous tests of the DRA on various disks and geometries, which are described in the report.
- The DRA has successfully identified relevant indication in numerous different disk geometries, including the JT8D turbine disk, Honeywell auxiliary power unit disks, and the F110 fan disk. This conclusion was drawn based on test results from numerous natural defects and ADs that were located in the disks provided by the customer.
- On another program with the Air Force Research Laboratory (AFRL) (FA8650-10-D-5210), the DRA was shown to provide a similar probability of detection (POD) as SIR

image interpretation by trained inspectors, meeting a goal of a_{90} of 40 mils. Appendix B reveals the POD results.

- The SIR Implementation Software Tool and Flowchart, developed under this contract, guides operators of an SIR system to a set of starting parameters for optimizing an inspection.
- A hybrid camera was developed that improves the documentation and data visualization capability of SIR. The favored approach was selected based upon simple optical comparison of overlaid images between the four configurations.
- An excellent level of synergism was developed between both this program and the AFRL program (FA8650-10-D-5210) that enabled both to reach further than if they were operated separately.
- Achieving all of the goals, stated above, moves the SIR technology forward and matures the platform.

7. REFERENCES

1. FAA Report. (2013). Focused Investigation for the Application of Sonic IR NDE Methods for the Detection of Service Induced Defects on Critical Rotating Components (DOT/FAA/TC-13/32).

2. Li, M., Holland, S. D., Meeker, W. Q., (2011). *Automatic Crack Detection Algorithm for Vibrothermography Sequence of Images*. Proceedings from the Review of Progress in Quantitative Nondestructive Evaluation, Kingston, RI.

3. Holland, S., (2012). Thermographic Signal Reconstruction for Vibrothermography, *Infrared Physics & Technology 54*(6), 503–511.

APPENDIX A—DRAWINGS AND LAYOUTS FOR ARTIFICIAL DEFECT INSTALLATION IN JT8D DISK

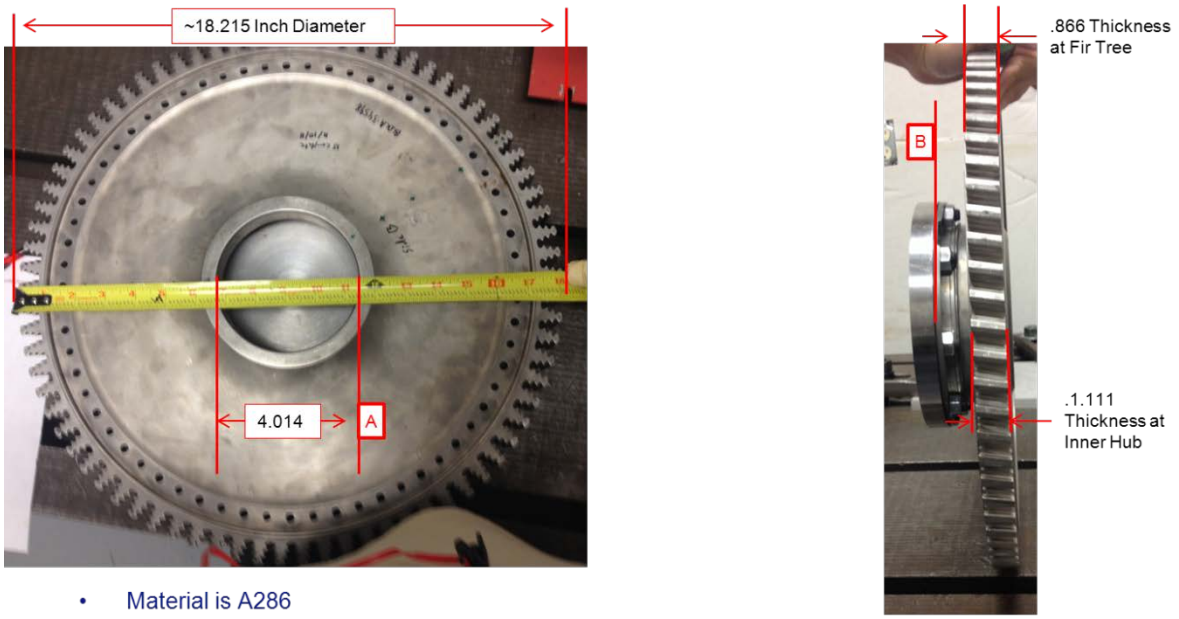

Figure A-1. Relevant disk information

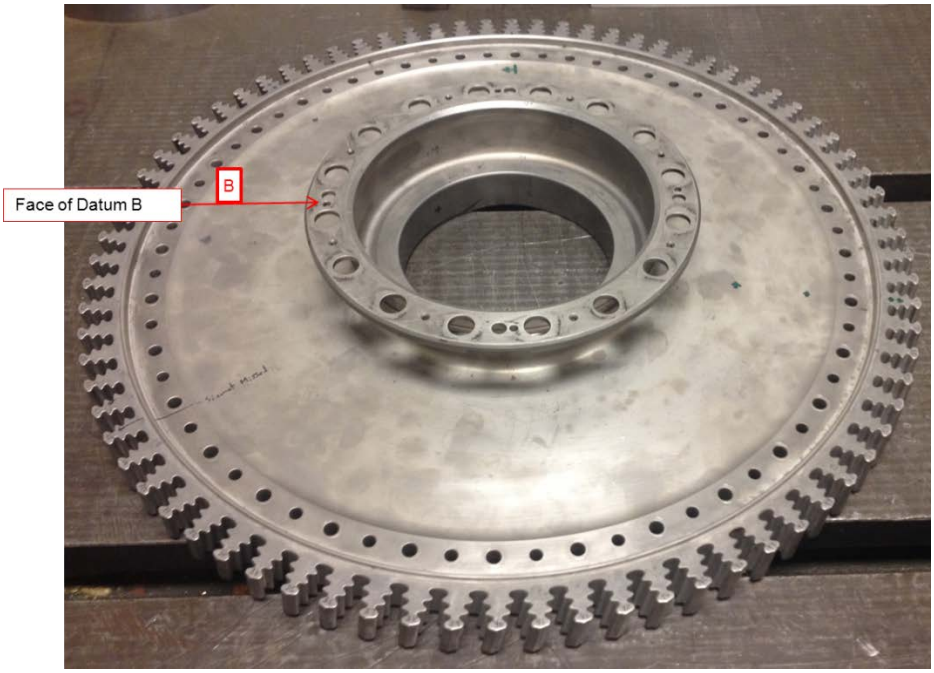

Figure A-2. AFT view of JT8D disk

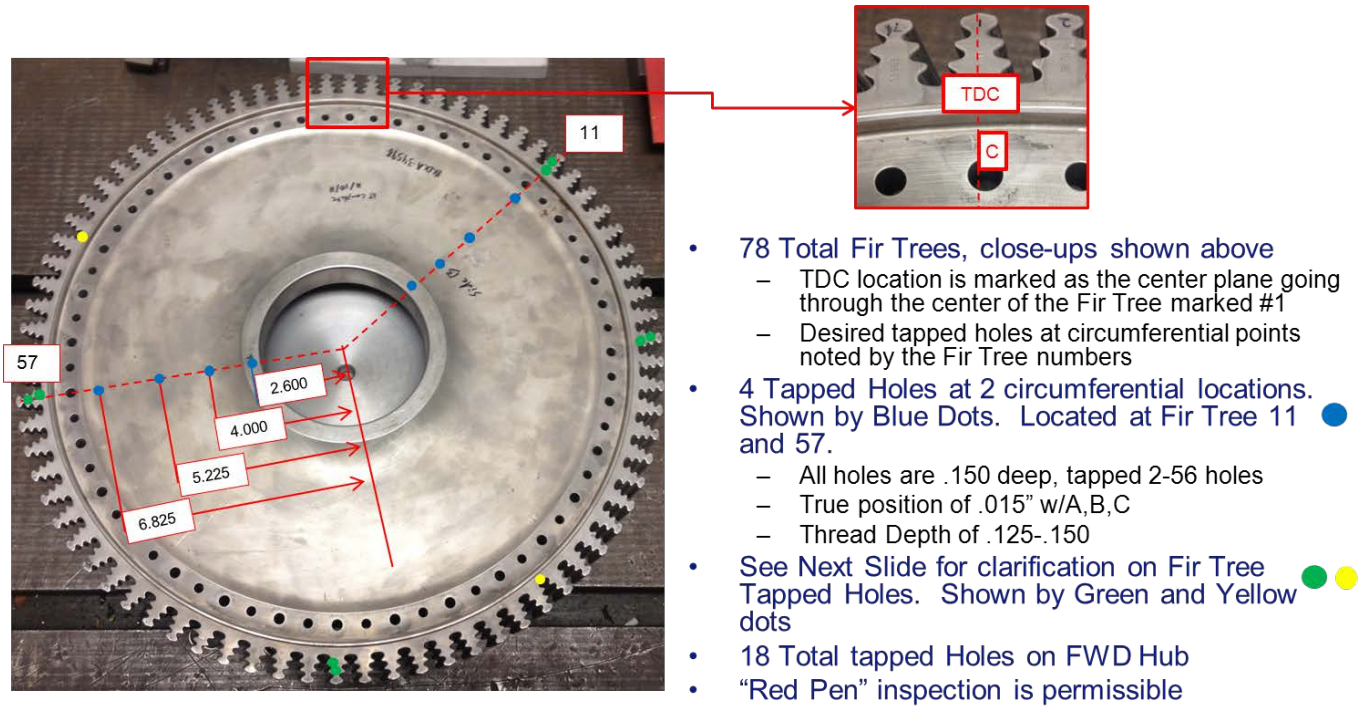

Figure A-3. Features on FWD face

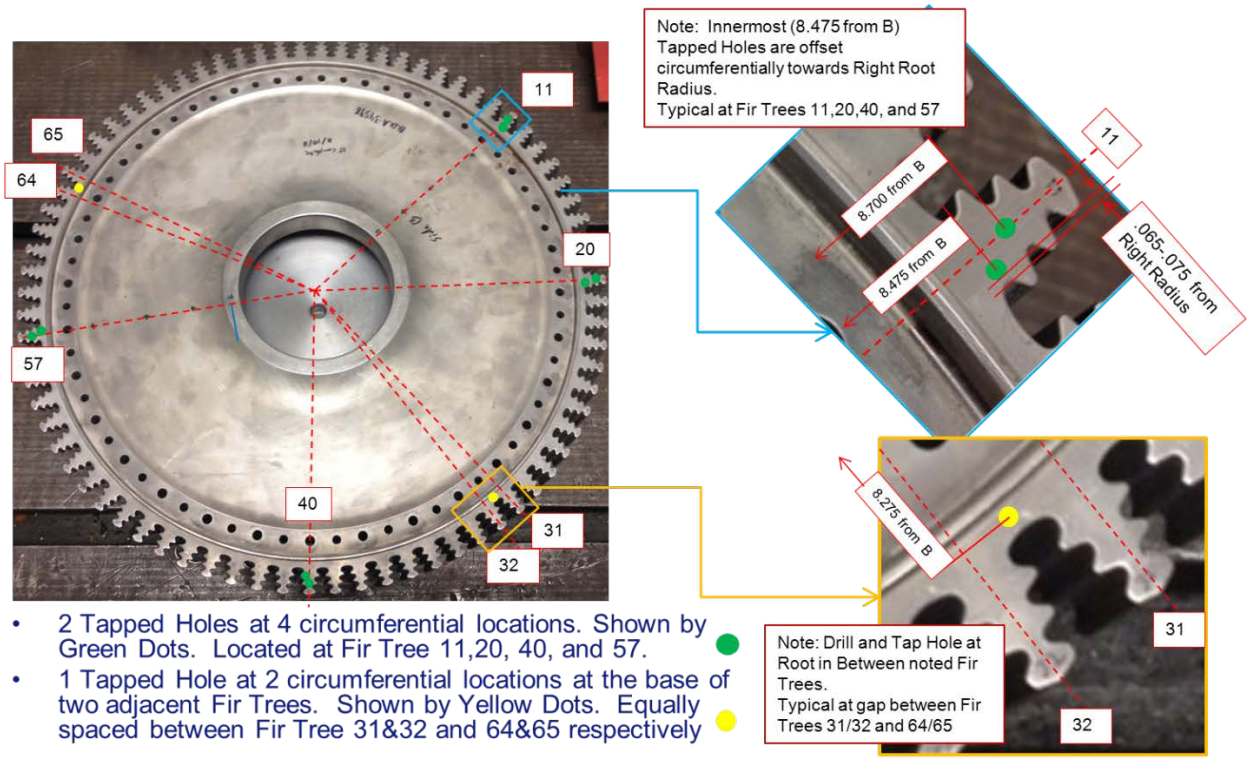

Figure A-4. Features on FWD face fir trees

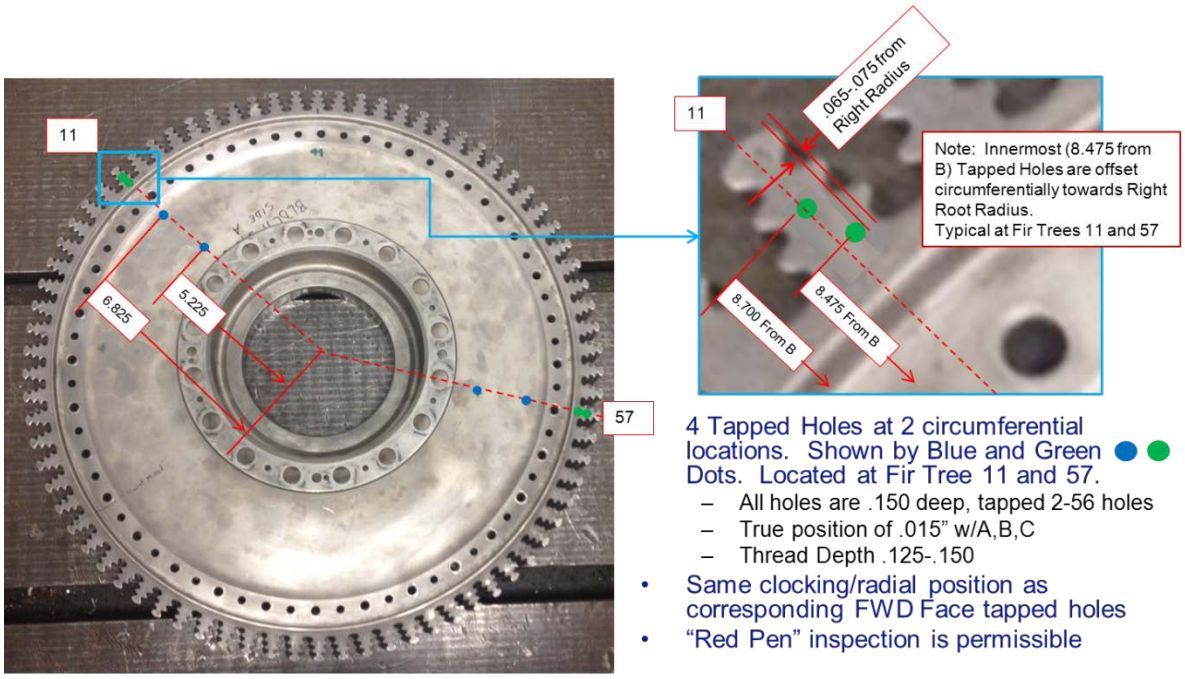

Figure A-5. Features on AFT face

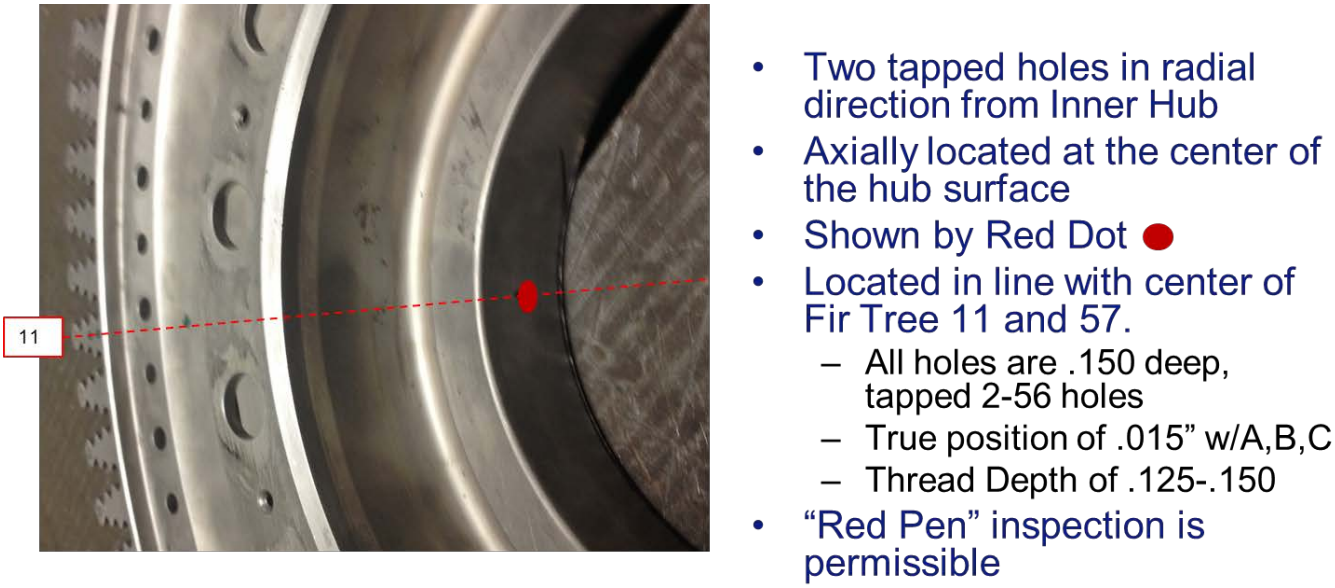

Figure A-6. Hub tapped holes

Note that the term hub refers to the bore of the disk.

APPENDIX B—EXAMPLE RESULTS OF DEFECT RECOGNITION ALGORITHM ON SONIC INFRARED INSPECTIONS

Figures B-1–B-6 are the defect recognition algorithm (DRA) results produced from various sonic infrared (SIR) inspections of various disk geometries. Most indications shown in the subsequent figures are thermo-mechanical fatigue (TMF) cracks, but the DRA was successful in identifying artificial defects (ADs) as well. See figure descriptions for details pertaining to the indications' origin: crack or AD.

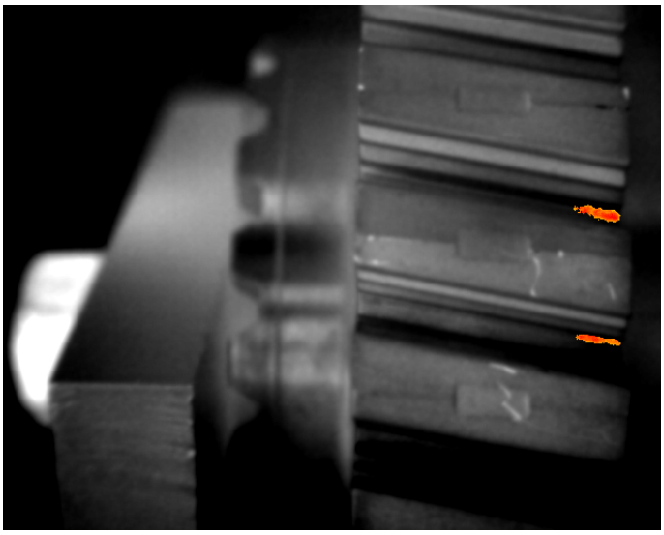

Figure B-1. Auxiliary power unit disk with DRA results revealing two TMF cracks

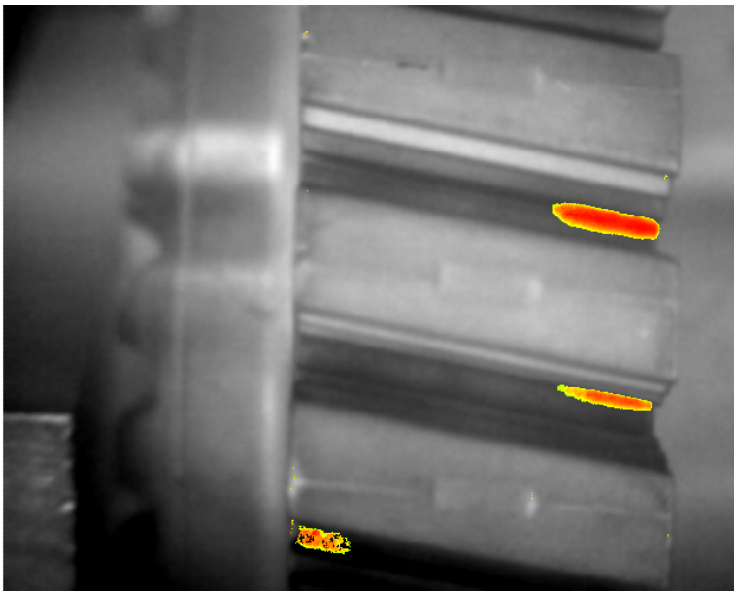

Figure B-2. Auxiliary power unit disk with DRA results revealing three TMF cracks

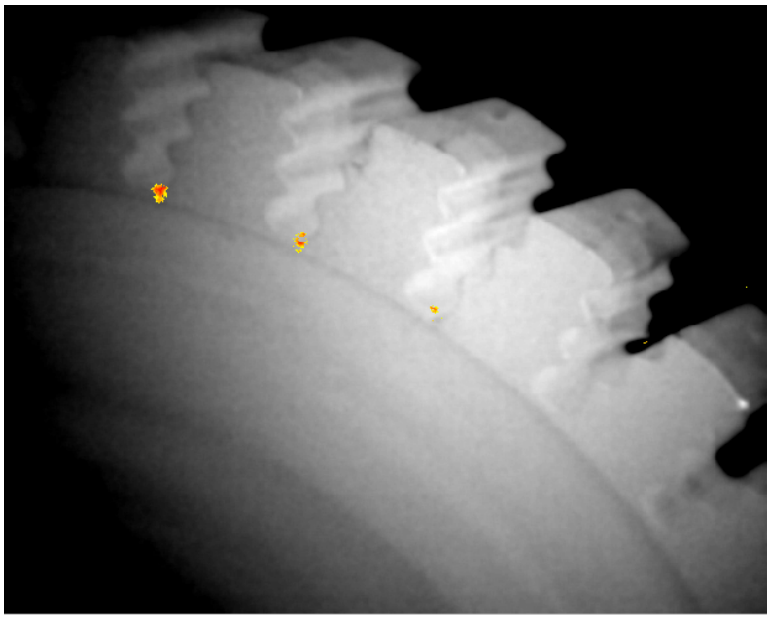

Figure B-3. Auxiliary power unit disk with DRA revealing three TMF cracks; isometric viewing angle

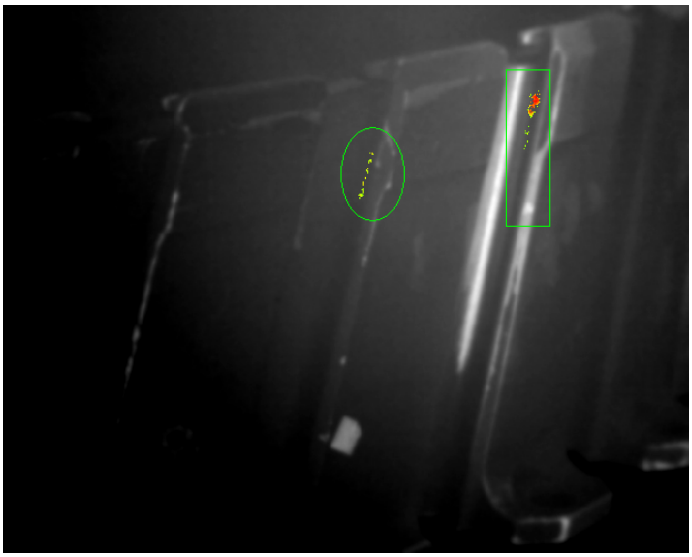

Figure B-4. F110 fan disk with DRA results revealing two fretting cracks; user-defined regions show; slot 20 and 21

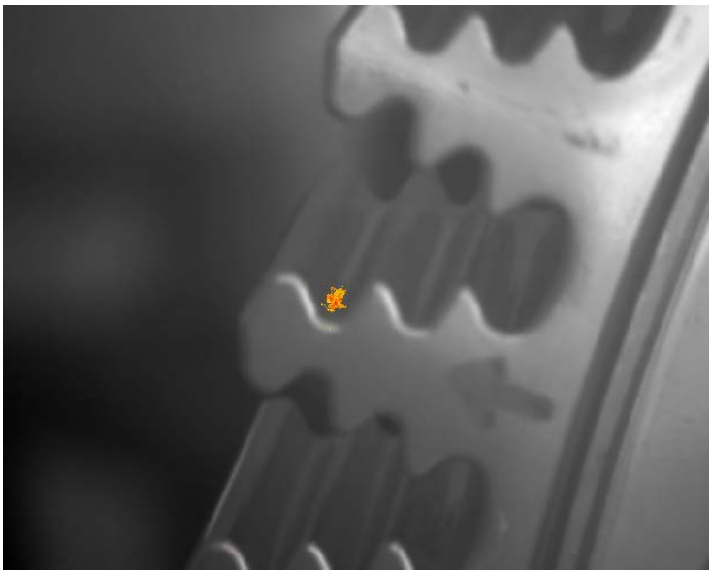

Figure B-5. JT8D turbine disk with DRA results revealing HCF crack

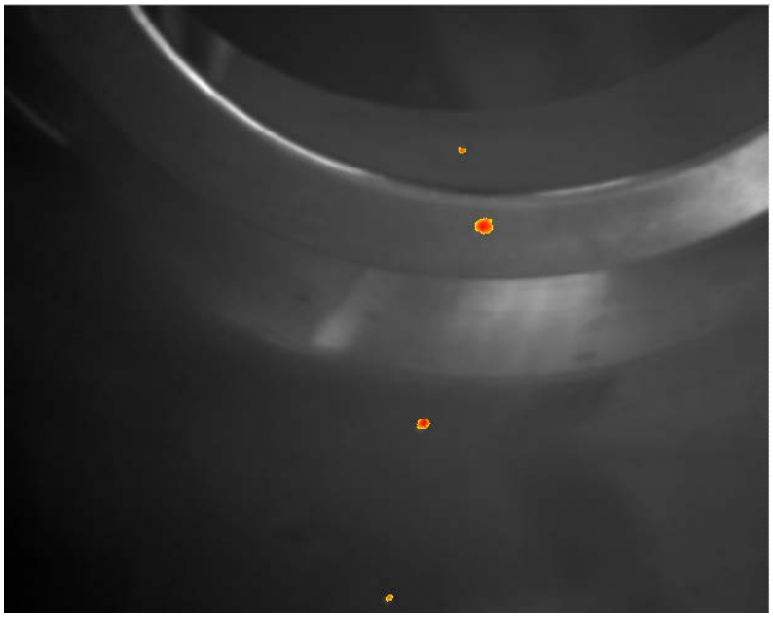

Figure B-6. JT8D turbine disk with DRA results revealing set screw AD's in Bore and web

The DRA was tested on two sets of probability of detection (POD) blade specimens. The purpose of the POD testing on blades was to gauge the performance of the DRA. This testing was performed under an Air Force Research Laboratory contract (FA8650-10-D-5210), and the data shown in figures B-7–B-9 have been cleared under the Clearance Case Numbers 88ABW-2015-4925 and 88ABW-2015-1270. The data in figures B-7 and B-8 show that the DRA performed statistically better than a minimally trained inspector. The DRA achieved an a_{90} of 39 mils and 45 mils for the two blade sets (note that 40 mils is the stringent requirement for fluorescent penetrant inspection on certain components). Experienced SIR inspectors were able to achieve an a_{90} of ~18mils, as seen in figure B-9. This shows that there is room for improvement in

the DRA, but this implementation is a quantitatively good first step by achieving an a_{90} or ~40 mils without any algorithmic optimization for blade components. The DRA was developed with disk SIR data, which appear to have less noise than blade SIR data because of the nature of their geometry and response to the acoustic chaos.

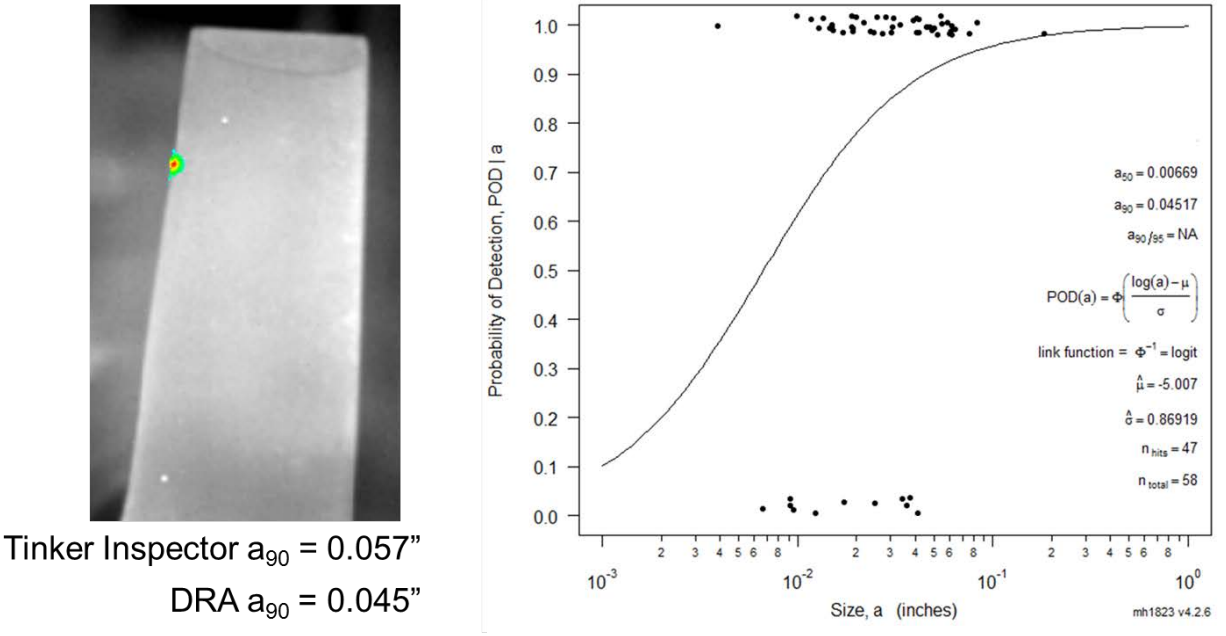

Figure B-7. The a_{90} (a) comparison to minimally trained inspector example DRA image and (b) DRA SIR POD for Blade Set #1, DRA POD Plot (Clearance Case Number 88ABW-2015-4925)

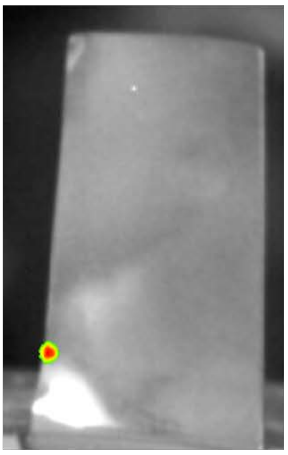

Tinker Inspector a_{90} = 0.041”

DRA a_{90} = 0.039”

(a)

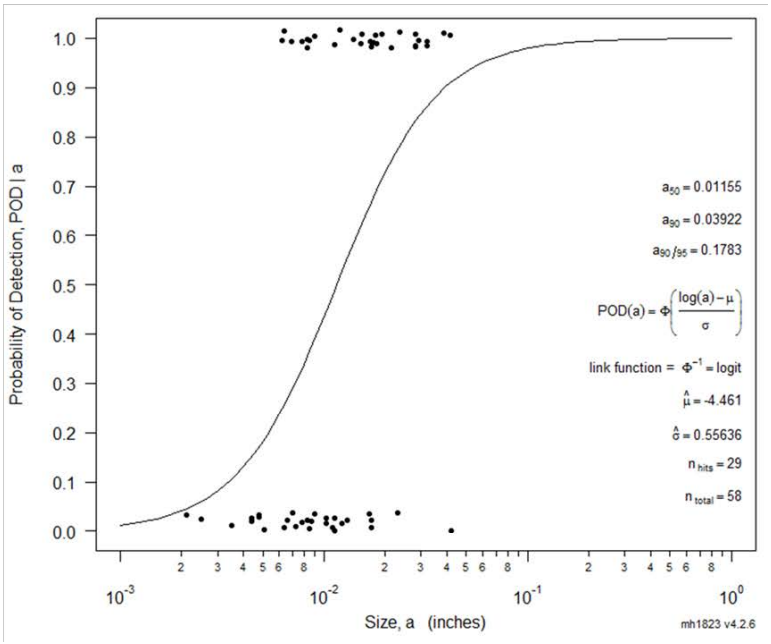

(b)

Figure B-8. The (a) a_{90} comparison to minimally trained inspector and example DRA image and (b) DRA SIR POD for Blade Set #2, DRA POD Plot (Clearance Case Number 88ABW-2015-4925)

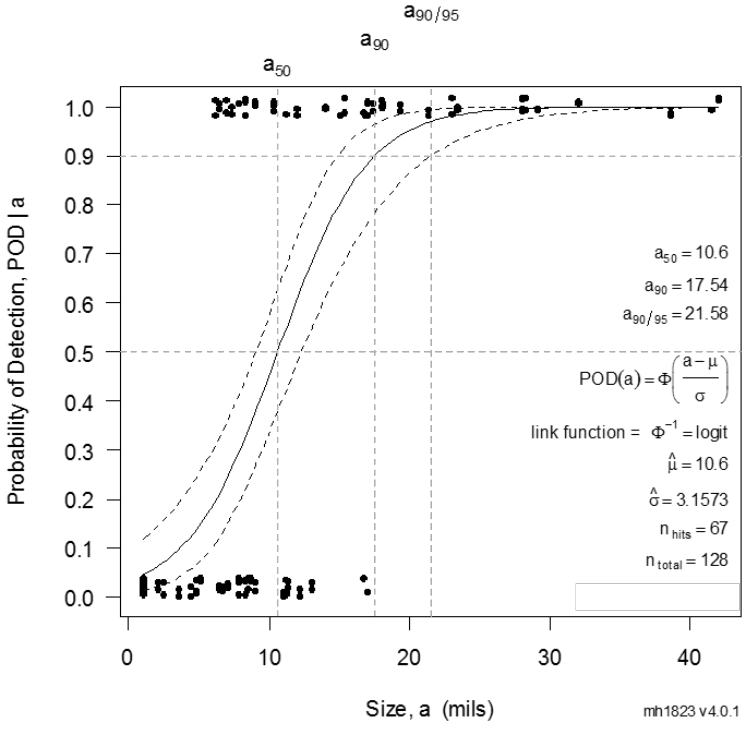

Figure B-9. SIR capability POD on Blades Set #2 with experienced inspectors (Clearance Case Number 88ABW-2015-1270)

APPENDIX C—EXAMPLE OF SONIC INFRARED IMPLEMENTATION TOOL REPORT

The sonic infrared (SIR) Implementation Tool generates a report with recommendations for settings and parameters of the SIR setup. The report also includes an image (which shows an example SIR setup) to add context to the recommendations in the report. The following is an example report generated by the SIR Implementation Software Tool:

SIR IMPLEMENTATION TOOL REPORT

SUMMARY:

Component:	Disk
Defect Type:	Cracks
Inspection view:	View Entire Component
Defect Size Range:	< 0.050"
Approximate Size of Inspection Area:	3-5"
Material of Component:	Titanium
Existing Attachment Areas for Fixture:	Yes
Areas of Contact Available:	Yes

RECOMMENDATIONS:
SIR is an inspection technology best suited for finding surface cracks.
You can inspect this component for cracks by following the content provided below.

Recommended IFOV: ~0.005″/pixel
IFOV = Instantaneous Field of View (resolution of camera: inches/pixel or pixels/inch)

Recommended # of inspection views to cover the inspection area: 2–3

Recommended Excitation Time: 0.50–1.0 seconds.
For larger, thicker, and heavier components, it is recommended that the excitation time be on the upper end of the recommended range: 0.75–1.0 seconds

Since there are existing attachment points, it is recommended that the fixture, used for inspecting the component, attach at the existing attachment points.

Given that there contact regions available, let the ultrasonic exciter impart energy through this area. Be sure to have flush contact between the exciter and the contact region.

Example of SIR inspection configuration

Figure C-1. Example SIR inspection configuration for disk